Applied Catalysis B: Environmental 96 (2010) 126–141

Contents lists available at ScienceDirect

Applied Catalysis B: Environmental

journal homepage: www.elsevier.com/locate/apcatb

The effect of Fe^{2+}, Fe^{3+}, H_2O_2 and the photo-Fenton reagent at near neutral pH on the solar disinfection (SODIS) at low temperatures of water containing *Escherichia coli* K12

Dorothee Spuhler, Julian Andrés Rengifo-Herrera, César Pulgarin *

Institute of Chemical Sciences and Engineering (ISIC), EPF Lausanne, CH-1015 Lausanne, Switzerland

ARTICLE INFO

Article history:
Received 26 November 2009
Received in revised form 1 February 2010
Accepted 4 February 2010
Available online 12 February 2010

SODIS
Iron
photo-Fenton
Escherichia coli K12
Photo-oxidative stress

ABSTRACT

The effect of Fe^{2+}, Fe^{3+}, H_2O_2 and the photo-Fenton system ($Fe^{2+\text{ or }3+}/H_2O_2/h\nu$) on solar water disinfection (SODIS) at low temperature and at near neutral pH are discussed in detail. We focus on *Escherichia coli* K12 suspended in either MilliQ water, water containing mineral ions and in MilliQ water enriched with resorcinol, a model for natural organic matter (NOM).

Recently, the photo-Fenton reagent at near neutral pH and at millimolar concentrations (0.6 mg $^{-1}$ $Fe^{2+\text{ or }3+}$ and 10 mg L^{-1} H_2O_2), was demonstrated to be highly efficient not only for the acceleration of solar disinfection of river water, but also for the elimination of NOM, which is a known precursor for halogenated disinfection byproducts.

In this work, these effects were systematically assessed at laboratory scale and in well controlled conditions excluding thermal inactivation. Besides the highly bactericidal properties of the photo-Fenton system at near neutral pH, a bactericidal effect of Fe^{2+} alone and of Fe^{3+} under irradiation ($Fe^{3+}/h\nu$) were also observed. This was associated with diffusion and intracellular dark Fenton reactions for Fe^{2+}, while the effect of $Fe^{3+}/h\nu$ was attributed to the adsorption of Fe^{3+} on the bacterial cell wall and subsequent photosensitization of these iron-bacteria exciplexes, leading to the direct oxidation of the cell membrane and the generation of ROS close to the target microorganism.

In MilliQ water, photo-inactivation rates for *E. coli* were increased by 200% in the presence of $Fe^{2+}/h\nu$ compared to the basic SODIS system ($h\nu$) and up to 250% in the presence of $Fe^{2+}/H_2O_2/h\nu$. When Fe^{3+} was added, photo-inactivation was enhanced up to 135% for $Fe^{3+}/h\nu$ and 145% for $Fe^{3+}/H_2O_2/h\nu$.

Inorganic ions contained in mineral water did generally inhibit the beneficial effect of $Fe^{2+\text{ or }3+}$ and H_2O_2 on bacterial inactivation. In contrast, the systems containing model NOM (resorcinol in MilliQ water, corresponding to 30 mg TOC L^{-1}) resulted in a higher iron-photo-assisted bacterial inactivation. This was associated with the formation of Fe^{3+}-organo bounds, which are stable at near neutral pH and undergo photosensitization under solar radiation leading to the generation of ROS and the oxidation of the organic compounds. Photo-inactivation in the presence of the photo-Fenton reagent was enhanced up to 320% for $Fe^{2+}/H_2O_2/h\nu$ and 355% for $Fe^{3+}/H_2O_2/h\nu$, with a simultaneous mineralization of 90% TOC within 4 h.

Based on these experimental results and supported by literature, a mechanistic interpretation of iron-catalyzed solar water disinfection is proposed, which illustrates the possible pathways involved in photo-inactivation of *E. coli* in the presence of Fe^{2+}, Fe^{3+} and H_2O_2.

1. Introduction

Today, still 1.1 billion people lack access to safe drinking water [1]. Safe drinking water and sanitation is the condition for physical health and intellectual, social and economical activity and development. To reach the millennium development goals, there is an urgent need for innovative drinking water treatment technologies, which require little or no energy, use locally available material and human resources and involve low maintenance costs. Solar Water Disinfection (SODIS) is such a simple and low-cost water treatment. SODIS is very promising for remote areas or urban slums in regions with consistently sunny climate. But also in emergency situation, SODIS can be a valuable alternative. Water is filled-up in 1–1.5 L polyethylenterephthalat (PET) bottles or plastic bags and exposed for 6 h by a solar intensity of about

* Corresponding author at: Institute of Chemical Sciences and Engineering (ISIC), Group of Electrochemical Engineering, EPF Lausanne, Station 6, CH-1015 Lausanne, Switzerland. Tel.: +41 21 693 47 20; fax: +41 21 693 31 85/47 22.
E-mail addresses: dorothee.spuhler@gmail.com (D. Spuhler), Cesar.Pulgarin@epfl.ch, julianandres.rengifo@gmail.com (C. Pulgarin).

0926-3373/$ – see front matter © 2010 Elsevier B.V. All rights reserved.
doi:10.1016/j.apcatb.2010.02.010

550 W m^{-2}[2]. The inactivation, or death if overexposure is reached, of pathogenic microorganism is caused by the synergistic effect of radiation and heat [3]. UVB light ($\approx$280–320 nm) is directly absorbed by the bacterial DNA leading to serious damage or inactivation [4]. Thermal inactivation occurs, when temperatures above 50 °C are reached [5,2]. Over 70% of inactivation, however, can be accounted to UVA and visible light (>320 nm) [3]. In this range photosensitizers (PS) get excited and react either directly with biomolecules or with surrounding oxygen, generating reactive oxygen species (ROS) such as $^1O2$, $O_2^{\bullet -}$, HO_2, H_2O_2 or $^\bullet$OH. PS can either be exogenous (e.g. humic acids) [3] or endogenous (e.g. cytochrome, flavin, etc.) [6,3,4,7]. Exogenous short-living ROS (e.g. $^\bullet$OH) damage membranes, while long-living ones (e.g. H_2O_2) diffuse into the cells. Endogenous long-living ROS directly damage cells (e.g. lipid peroxidation) or generate more reactive and short-living ROS such as $^\bullet$OH inside the cells. $^\bullet$OH reacts at almost diffusion controlled rate with cellular biomolecules and when $^\bullet$OH enters in contact with DNA, strands breaks, nucleic base modifications and serious damage occurs [8,9].

As SODIS requires a consequent incident solar radiation and water temperature rise, this process is strongly climate-dependent and only small volumes can be treated at a time. The control of the required exposure time for a given weather condition and water source can overburden some households, leading to underexposure, regrowth and limited acceptance among the population [10].

During the past 20 years, the physical improvement of SODIS (e.g. black backs) [11], the possibility of adding a photocatalyst (e.g. TiO_2) [12–16] or an artificial PS (e.g. methylene blue) [2], have been assessed.

Recently the photo-Fenton system ($Fe^{3+}/H_2O_2/h\nu$) was observed to speed-up the solar photo-inactivation of *Escherichia coli* at near neutral pH [17–21] and to degrade natural organic matter (NOM) [22,23,21,24], which is often responsible for regrowth or halogenated disinfection byproducts.

The Fenton reagent involves basically the formation of highly reactive $^\bullet$OH via the Haber–Weiss reaction [25,26]:

$$Fe^{2+} + H_2O_2 \rightarrow Fe^{3+} + {}^\bullet OH + OH^- \quad k = 50\text{–}80\ M^{-1}\ s^{-1} \tag{1}$$

Today, the Fenton reagent is widely applied in the oxidation of biorecalcitrant organic water pollutants [27,28]. But the Haber–Weiss reaction (Eq. (1)) is also of biological relevance because for most living organisms, the alteration of the intracellular concentration of Fe^{2+} and H_2O_2 can increase the intracellular formation of $^\bullet$OH, leading to DNA and cell damage [29].

In the Fenton reagent, Fe^{2+} can be regenerated from Fe^{3+} in the presence of H_2O_2 (Fenton-like reactions) [26,28]:

$$Fe^{3+} + H_2O_2 \rightarrow Fe^{2+} + HO_2{}^\bullet + H^+ \tag{2}$$

But as the rate constant k in Eq. (2) is considerably lower (approximately 10^{-6} to $10^{-2}\ M^{-1}\ s^{-1}$) [25,26,30–32] than for Eq. (1), this reaction is the limiting step for the Fenton reagent.

The irradiation of the system (photo-Fenton systems) is highly beneficial because some Fe^{3+}-hydroxy complexes undergo photoreduction under UVA and visible radiation, producing $^\bullet$OH and regenerating Fe^{2+} via ligand to metal charge transfer (LMCT). The process pH was until now generally perceived as the limiting factor for photo-Fenton systems, because $FeOH^{2+}$, the most photo-active Fe^{3+}-hydroxy complex which overlaps with the solar UV spectrum, is predominant at low pH ($\approx$2.8) [33,27,28]. The photo-activity of $FeOH_2{}^+$, which is the predominant species at higher pH, has not been quantified but appears to be much lower [34].

Fe^{3+}-organo complexes, which absorb light in the solar spectrum and are stable at environmental pH allow to circumvent pH dependency of traditional photo-Fenton systems. Strong and photoactive complexes with Fe^{3+} are formed by carboxylate groups or polycarboxylates (e.g. oxalate, malonate, and citrate), the most common functional groups of dissolved NOM [28,35–37]:

$$[\text{R-COO}^- - Fe^{3+}]^{2+} \xrightarrow{h\nu} Fe^{2+} + CO_2 + R^\bullet \tag{3}$$

Depending on the type of the ligand and pH, high-valent oxo-iron species (ferryl, Fe(IV)=O) can also be involved in the radical formation and decomposition of organic compounds in photo-Fenton systems [26,38,28,24].

Until now, the enhancement of bacterial photo-inactivation via photo-Fenton at near neutral pH was reported at lab scale, pilot scale and in natural waters at reagents concentrations in the micro to millimolar range [18–21]. Further, disinfection via an iron/oxalate system [17], via photo-Fenton at pH 4 [39] or an immobilized photo-Fenton reagent on structured silica surfaces [40] has also been reported.

In this paper, we carried out a systematic study, investigating the effect of Fe^{2+}, Fe^{3+} and H_2O_2 on the photo-inactivation of *E. coli* in MiliQ water, mineral water and MilliQ water enriched with resorcinol, a model NOM. Based on our experimental results and literature reports, we suggest a mechanistic interpretation of the differences in how Fe^{2+}, Fe^{3+}, H_2O_2 and the photo-Fenton reagent affect bacterial photo-inactivation.

Iron-catalyzed solar drinking water disinfection is a novelty from a scientific and technological point of view. The application of photo-Fenton to SODIS could take advantage of iron naturally present in raw drinking water and would allow to treat faster larger volumes of water and limit the risk of bacterial regrowth. Moreover, the photo-Fenton system could simultaneously eliminate xenobiotics and chemical pollutants such as pesticides [41,42] and arsenic [43,38,44] or NOM [12,23], without the risk of the formation of toxic halogenated disinfection byproduct [45].

To our knowledge, this is the first report of a systematic study on photo-Fenton solar water disinfection allowing a mechanistic interpretation and which illustrates the possible pathways involved in photo-inactivation of *E. coli* in the presence of Fe^{2+}, Fe^{3+}, H_2O_2 and the photo-Fenton reagent.

2. Materials and methods

2.1. Chemicals and reagents

All chemicals were reagent grade, used as received and supplied by Sigma–Aldrich or Fluka (Steinheim, Germany). Pure water was analytical grade from a Millipore Elix 3 system combined to a prograd filter (Millipore AG, Zug, Switzerland). Glassware for analytical analysis and reactors were acid soaked after every experimental series in order to prevent iron cross-contamination (10% HCl, 3 days and nights).

2.2. Analytical methods

2.2.1. Dissolved

$Fe^{2+\ or\ 3+}$ Dissolved iron ($Fe^{2+\ or\ 3+}$) was measured by the Ferrozine method. Samples were filtered (0.45 μm) to eliminate bacteria previous to measurement. For 1.6 mL of sample, 0.2 mL of a Ferrozine solution (4.9 mM) was added, where after coloring rapidly occurred in the presence of Fe^{2+}. Then, 0.2 mL of Hydroxylamine Hydrochloride (10% w/w) was added in order to reduce Fe^{3+} to Fe^{2+}. The final coloration was measured after a reaction time of 20 min [46]. 0.5 mL acetate buffer solution (pH 4.65) were added for a final pH of 4.5–5 [47]. Absorbance was measured at 562 nm and 25 °C by photospectrometry (Lambda 25 UV/Vis Spectrometer, PerkinElmer, Morens, Switzerland) and than related to corresponding $Fe^{2+\ or\ 3+}$ concentrations by a calibration

curve over 10 points ($R^2 > 0.95$) [47,46]. The standard solution for calibration were prepared with $FeSO_4 \cdot H_2O$.

2.2.2. Total iron

Total iron was measured with atomic absorption (AAnalyst 400, PerkinElmer, Morens, Switzerland). The calibration (10 points) solutions were prepared with $Fe(NO_3)_3$.

2.2.3. Total organic carbon

Total organic carbon (TOC) was monitored by catalytic oxidation/NDIR combustion (TOC-VCS/N standard model, SHIMADZU Schweiz GmbH, Reinach, Switzerland) combined with an automatic sample injector (ASI-V, SHIMADZU Schweiz GmbH, Reinach, Switzerland). A three point calibration curve for 20 ppm was used. In the presence of H_2O_2, this was first neutralized with $NaHSO_3$. As it turned out that the addition of $NaHSO_3$ induced acidification affecting the stability of the samples after withdrawing, samples were stored at −20 °C immediately and no $NaHSO_3$ was added. The samples were defrosted just before measurement.

2.3. Microbial methods

2.3.1. Bacterial strains

The *E. coli* strain K12 (MG1655) was used for all here presented results and supplied by the Deutsche Sammlung von Mikroorganismen und Zellkulturen (DSMZ, German Collection for Microorganisms and Cell cultures, Darmstadt, Germany). *E. coli* K12 is a non-pathogenic and approximates of wild-type *E. coli*, a typical indicator bacteria for enteric pathogens.

2.3.2. Sample preparation

Strain samples were stored in cryo-vials containing 20% glycerol at −20 °C. Bacterial pre-cultures were prepared for each experimental series by streaking out a loopfull from the strain sample onto Plate Count Agar (PCA) and subsequent incubating the plates for 24 h at 37 °C (Heraeus Incubator B 5060 EK-CO2, Heraeus Instruments, Hanau, Germany). From the growing colonies, one was re-plated on a separate PCA and incubated again for 24 h at 37 °C.

Luria-Bertani (LB) broth (10 g Bacto™ Trypton, 5 g Yeast extract, 10 g NaCl per liter) was prepared for each experimental series by suspension in MilliQ water and heat-sterilization by autoclaving at 121 °C for 20 min (VST 500A, LS SECFROID, Blanc Labo, Lonay, Switzerland).

To prepare the bacterial pellet for the photo-inactivation experiments, one colony was picked from the pre-cultures and loop-inoculated into a 50 mL sterile PE Eppendorf flask containing 5 mL of LB broth. The flask was then incubated at 37 °C and 180 rpm in a shaker incubator (Minitron AI 71, INFORS AG, Bottmingen, Switzerland). After 8 h, cells were diluted (1% v/v) in a 250 mL Erlenmeyer flasks containing 25 mL of prewarmed LB broth and incubated at 37 °C for 15 h in the Heraeus Incubator (B 5060 EK-CO2, Heraeus Instruments, Hanau, Germany) until stationary physiological phase was reached. Bacterial growth and stationary phase was monitored by optical density at 600,nm.

Cells were harvested during stationary growth phase by centrifugation (15 min at 5000 × *g* RCF and 4 °C) in a universal centrifuge (HERMLE Z 323 K, Renggli Laboratory Systems, Renens, Switzerland). The bacterial pellet was resuspended and washed for 10 min in the centrifuge. Washing was repeated twice and the final pellet was resuspended to the initial volume. This procedure resulted in a bacterial pellet of approximately 1.5×10^8 CFU mL^{-1}. Washing and resuspension was done either in heat-sterilized MilliQ water, a saline solution (NaCl/KCl), a nutritional solution containing Bacto™ Trypton or mineral water (Alpina, Coop, Switzerland).

In the case of saline solution, the experimental concentrations in the reactors were 0.8 mg NaCl L^{-1} and 0.08 mg KCl $^{-1}$ in the photo-inactivation experiments and 0.8 g NaCl $^{-1}$, respectively 0.08 g KCl L^{-1} for the determination of iron in the different experimental compartments. In the case of trypton, concentrations were 0.1 and 1 g $^{-1}$ for the two experiments respectively. Resorcinol, which was used to simulate model organic matter was added at concentration of 30, respectively 60 mg L^{-1} for each experiment.

In the beginning of each experiment the reactors containing the bacterial suspension were placed in the dark solar simulator at 25 °C under magnetic stirring for at least 1 h in order to let bacteria adapt to the new matrix and to allow die-off of the most stress sensitive species. After stabilization of the population, the reagents ($FeSO_4$, $FeCl_3$, H_2O_2) were added before turning on the lamp.

2.3.3. Plating

Colony forming units (CFU) were monitored by pour-plating on PCA. At each data point, 1 mL of sample was withdrawn. Exceeding H_2O_2 was neutralized with catalase, samples were diluted in 10% steps and poor plated on PCA. Plates were incubated for 24 h at 37 °C and the CFU were counted manually.

2.4. Experimental

2.4.1. Photo-inactivation experiments

Six circular Pyrex reactors (4 cm × 9 cm, 100 mL, home fabric, verrerie du Jorat, Switzerland) were placed on a rectangular magnetic stirrer (six places, home fabric, ISIC, EPFL, Switzerland) in a solar simulator (CPS Suntest System Heraeus Noblelight, Hanau, Germany, maintained by Atlas Material Testing Technology LLC, Härkingen, Switzerland). The Suntest system contained a basic uncoated quartz glass light tube a filter E and an IR screen (simulation of solar global radiation outdoors daylight). Under these conditions the emitted radiation corresponds to about 0.5% of total photons emitted at wavelength shorter than 300 nm (UVC and UVB range). The spectrum 300 nm follows the natural solar spectrum. Temperature in the reactors did never exceed 38 °C. The radiation intensity was 550 W m^{-2} (Fig. 1) and were monitored by a combination of a UV radiometer and a pyranometer connected to a data-logger (CUV3 and CM6b respectively, Kipp & Zonen, Delft, Holland).

Initial bacterial populations were 10^6 to 10^7 CFU mL^{-1}. $Fe^{2+ \text{ or } 3+}$ and H_2O_2 concentrations were 0.6 mg L^{-1} respectively 10 mg L^{-1}. These concentrations were determined experimentally as being optimal (results not shown) and correspond to the limit, where bacterial inactivation cannot be further enhanced if more $Fe^{2+ \text{ or } 3+}$ were added.

Six systems were tested for the photo-inactivation effect on *E. coli* ($h\nu > 290$ nm): Fe^{2+}/H_2O_2 (**I**); Fe^{2+} (**II**); Fe^{3+}/H_2O_2 (**III**); Fe^{3+} (**IV**); H_2O_2 (**V**); $h\nu$ only (**VI**). An additional reactor was monitored on a separate magnetic stirrer in parallel and at same oxygenation and temperature levels, but strictly protected from radiation by an aluminum foil (dark control).

Seven experimental series were conducted and each was repeated at least three times. The first to fourth series allowed to determine the ideal experimental conditions. The first was conducted under irradiation with bacteria resuspended in saline solution, leading to concentrations of 0.8 mg NaCl L^{-1} and 0.08 mg KCl L^{-1} respectively in the reactors. The second series used the same experimental conditions in a dark run. The third and forth series was conducted with bacteria resuspended in trypton, a nutrient based on peptides, under irradiation and in the dark (0.1 g trypton L^{-1}). The fifth, sixth and seventh series of experiments were all carried out with bacteria prepared in MilliQ water and under irradiation ($h\nu > 290$ nm) in either MilliQ water (pH 5–5.5),

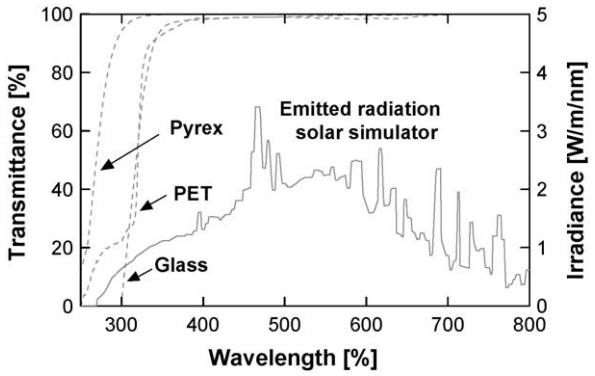

Fig. 1. Emitted spectrum (W m^{-2} nm^{-1}) by the solar simulator in the range of 250–800 nm (—) and the transmittance (%) of different reactor Materials (- - -). The radiation below 300 nm (UVC/UVB) corresponds to about 0.5% of total emitted photons. Approximately 7% are emitted between 300 and 400 nm (UVB/UVA). The profile of the photons emitted between 400 and 800 nm follows the solar spectrum, but because of a special IR filter, temperature in the reactors did never exceed 38 °C. The total radiation intensity was 550 W m^{-2}.

mineral water (pH 7–7.5) or MilliQ water enriched with resorcinol, a model natural organic matter (pH 5–5.5).

The results and discussion parts of the present paper were based on the three last experimental series. The results from the experiments with saline solution and trypton are not discussed explicitly. However, under irradiation, the observed inactivation rates were not considerably affected by the small amount of NaCl/KCl (0.8 and 0.08 mg L^{-1} respectively) in the bacterial suspensions (compare MilliQ and Saline in Table 2). Therefore the results obtained in the dark saline experiment were used to explore the comportment of the MiliQ experiment in the dark. The results from the experiments with trypton are used to provide the evidence about the reactions involving $Fe^{2+}/H_2O_2/h\nu$, $Fe^{2+}/h\nu$, $H_2O_2/h\nu$ in the dark in the presence of organic compounds.

2.4.2. Post-irradiation events

Regrowth after 24 and 48 h in the dark was measured for the experiment in MilliQ water and mineral water. Samples were withdrawn after 60, 120 and 240 min in the case of MilliQ and after 0, 90 and 300 min for the experiment carried out in mineral water. The samples were directly introduced into sterile 10 mL Eppendorf flasks having air in half of the volume. In the presence of H_2O_2, the samples were taken in two parts, one part was neutralized for excess H_2O_2, the other was left untouched. Samples were then placed for either 24 or 48 h in the dark at 25 °C before measurement of CFU by pour-plating on PCA. For the final plating, remaining H_2O_2 was always inactivated with catalase.

2.4.3. Iron concentration in the different compartments of the experimental suspension

Bacteria suspensions were either prepared with MilliQ, saline solution or trypton, leading to concentrations of 10^7 to 10^8 CFU mL^{-1} and 0.8 g NaCl L^{-1}, 0.08 g KCl L^{-1} and 1 g trypton L^{-1}. H_2O_2 concentrations were 20 or 30 mg L^{-1} and irradiation was kept constant for either 30 or 45 min. The pH was between 5 and 5.5 and temperature did not exceed 38 °C. To separate the different reactor compartment, 40 mL of sample were centrifuged during 20 min (5000 × *g*, 4 °C). 30 mL of the supernate were used to determined iron in the solution without bacteria. The other 10 mL containing bacteria, were used for resuspension of the bacterial pellet. This bacterial resuspension was either digested and iron was measured by the Ferrozine method or it was dispersed by ultrasound (Ultrasonic Cleaner, Branson 1200, Bender & Hobein, Zrich, Switzerland) and acidified for determination of iron by atomic absorption.

2.5. Data treatment and analysis

Solar bacterial inactivation depends on irradiance (W m^{-2}) and dose (W m^{-2} × time(s) = J m^{-2}). All our experiments were carried out under continuous irradiation at constant intensity. Therefore, experimental data are expressed as the measured colony forming units over time (CFU mL^{-1} vs. time). As temperature did never exceed 38 °C and thermal bacterial inactivation can be excluded beneath 45 °C, raw data was approximated by Chicks law [48]:

$$N_t = N_0 e^{-kt} \tag{4}$$

where N_0 is the number density of individuals prior to irradiation ; t is the irradiation time (at constant fluence rate); N_t is the number density of survivors at irradiation time t and k is the time based inactivation constant. This exponential results can be plotted by a straight line in semi-log graph. To compare inactivation under different conditions, first-order rate constants were obtained from the fitting of plots of log(CFU mL^{-1}) vs. time, and are reported as k_{obs} [min^{-1}]. The fitting was carried out by the method of least squares (95% confidence interval) and weighted by the standard deviation for minimal triplicate measurement in Matlab (MathWorks™). In systems, where the inactivation was better approximated by a two-phase exponential approach, two different first-order k_{obs} for each phase were determined and their time weighted average was calculated for the qualitative interpretation of data. For the fitting confidence interval of 95%, the variations of k_{obs} did not exceed 15%.

To identify with more evidence the beneficial effect of photo-Fenton systems ($Fe/H_2O_2/h\nu$) synergistic factors were calculated as follows:

$$S_{Fe/H_2O_2/h\nu} = \frac{k_{obs}^{Fe/H_2O_2/h\nu}}{k_{obs}^{(Fe+H_2O_2)/h\nu}} \tag{5}$$

$$k_{obs}^{(Fe+H_2O_2)/h\nu} = k_{obs}^{Fe} + k_{obs}^{H_2O_2/h\nu} \tag{6}$$

$$k_{obs}^{Fe} = k_{obs}^{Fe/h\nu} - k_{obs}^{h\nu}. \tag{7}$$

3. Results

Three experiments, which were carried out in the presence of ($h\nu$ >290 nm) for *E. coli* suspended in MilliQ water (pH 5–5.5), Mineral Water (pH 7–7.5) or MilliQ water enriched with resorcinol, a model organic compound (pH 5–5.5), are discussed here in detail. The photo-inactivation effect of six systems (plus optionally a dark control) were assessed: Fe^{2+}/H_2O_2 (**I**); Fe^{2+} (**II**); Fe^{3+}/H_2O_2 (**III**); Fe^{3+} (**IV**); H_2O_2 (**V**); $h\nu$ or dark only (**VI**); dark control. To analyze our results, the observed inactivation rates k_{obs} for a log-linear one-term exponential fit at constant radiation intensity were calculated. The k_{obs} are presented in Table 2.

3.1. Photo-inactivation in MilliQ water

Raw data of measured inactivation (markers) and first-order exponential fittings used to calculate k_{obs} are shown in Fig. 2. In the absence of light (dark control), the bacterial population remained stable within the experimental period of 4 h. However, during dark storage posterior to irradiation experiments in MilliQ water (results not shown), delayed inactivation within 48 h always occurred, probably due to osmotic stress in MilliQ water. Over 4 h, $k_{obs}^{h\nu}$ (0.06 min^{-1}, **VI**, Table 2) lies in the range of commonly published solar inactivation rates for *E. coli* [49]. The ranking for the different k_{obs} was: $Fe^{2+}/H_2O_2/h\nu > Fe^{3+}/H_2O_2/h\nu > Fe^{2+}/h\nu$

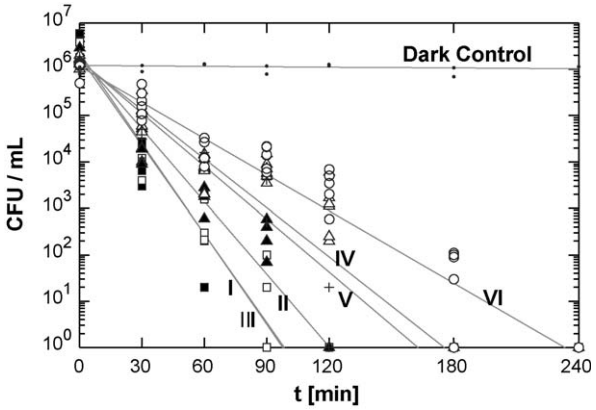

Fig. 2. Fenton-assisted photo-inactivation ($h\nu > 290$ nm) of *E. coli* suspended in MiliQ water (pH 5–5.5). Bacterial cells were harvested from stationary phase, washed and resuspended in the reactors. After acclimation, $Fe^{2+\ or\ 3+}$ and H_2O_2 were added to the corresponding systems. Remaining H_2O_2 was eliminated by catalase before plating. Markers represent raw data and lines show the resulting curve of a one-order exponential fitting (Matlab). Calculated observed inactivation rates are displayed in Table 2. The evolutions of $Fe^{2+\ or\ 3+}$ were measured simultaneously and except for system **II**, were iron concentration were measurable up to almost 100% to the beginning and the end of the experiment, iron was not detected in the samples after filtration. (**I**) (■) – 0.6 mg Fe^{2+} L^{-1}, 10 mg H_2O_2 L^{-1}; (**II**) (□) – 0.6 mg Fe^{2+} L^{-1}; (**III**) (▲) – 0.6 mg Fe^{3+} L^{-1}, 10 mg H_2O_2 L^{-1}; (**IV**) (△) – 0.6 mg Fe^{3+} L^{-1}; (**V**) (+) – 10 mg H_2O_2 L^{-1}; (**VI**) (○) – $h\nu$ only; (**VII**) (·) – dark control (*E. coli* only).

v > $H_2O_2/h\nu$ > $Fe^{3+}/h\nu$ > $h\nu$ only. The $H_2O_2/h\nu$ system enhanced the inactivation as k_{obs} was 145% of $k_{obs}^{h\nu}$. Exposure to the system $Fe^{3+}/h\nu$ resulted in an increase in bacterial photo-inactivation up to 135% while for Fe^{2+}/h v, the enhancement was 200%. Both photo-Fenton systems ($Fe^{2+}/H_2O_2/h\nu$ and $Fe^{3+}/H_2O_2/h\nu$), showed similar inactivation rates, which were about 250%, respectively 245% of $k_{obs}^{h\nu}$. Consequently, the synergistic factor $S_{Fe^{2+}/H_2O_2/h\nu}$ was approximately 1, while $S_{Fe^{3+}/H_2O_2/h\nu}$ was 1.4.

Except for system $Fe^{2+}/h\nu$, iron was not detected after filtration of the samples, and no correlation was established between inactivation rates and measured dissolved iron after filtration.

During 4 h in the presence of Fe^{2+}/H_2O_2/dark and H_2O_2/dark, the variation in bacterial population was <5% (Table 2, Saline dark). However, in the presence of Fe^{2+}/dark, an inactivation of 15% of k_{obs} for $Fe^{2+}/h\nu$ was observed.

Table 1
Chemical composition of Alpina mineral water (Coop, Switzerland). Analyzed the 26 of October 2005 by the Food Security office, Kanton Graubünden, Switzerland.

	Element					
	Na	K	Mg	Ca	Fe	F
mg L^{-1}	65.5	4.4	48.7	157.7	<0.005	0.23
mM L^{-1}	2.85	0.11	2.0	3.93	0	0.01
	Element					
	Cl	HCO_3^-	SO_4^-	NO_3^-	$Si(OH)_4$	
mg L^{-1}	65.5	770.1	90.4	1.3	40.7	
mM L^{-1}	0.26	12.0	0.94	0.91	0.42	

3.2. Photo-inactivation in the presence of inorganic ions (mineral water)

The composition of the used mineral water is shown in Table 1 and the results of the photo-inactivation experiments are displayed in Fig. 3 and Table 2. In the absence of osmotic stress, overall inactivation rates were lower than in MilliQ water. But k_{obs} in the presence of $h\nu$ only (0.048min^{-1}, **VI**, Table 2) was still in a common range and the difference to k_{obs} for $h\nu$ only in MilliQ water experiment was within the deviation for the 95%. The ranking for this experiment according to k_{obs} was: $Fe^{3+}/H_2O_2/h\nu > Fe^{2+}/H_2O_2/h$ v > $Fe^{2+}/h\nu > h\nu$ only > $H_2O_2/h\nu > Fe^{3+}/h\nu$. In contrast to the experiment in MilliQ, the presence of H_2O_2 did not enhance the photo-inactivation and even reduce it (85% of $k_{obs}^{h\nu}$). Neither did the presence of Fe^{2+} (90% of $k_{obs}^{h\nu}$) or Fe^{3+} (67% of $k_{obs}^{h\nu}$) alone (**V**, **II** and **IV**, Fig. 3 and Table 2).

The photo-Fenton systems ($Fe^{2+}/H_2O_2/h\nu$ and $Fe^{3+}/H_2O_2/h\nu$) accelerate photo-inactivation despite the unfavorable pH (7–7.5) up to 120%, respectively 150% and synergistic factors were higher than 1 ($S_{Fe^{2+}/H_2O_2/h\nu} = 1.7$, $S_{Fe^{3+}/H_2O_2/h\nu} = 2.92$).

3.3. Post-irradiation events in mineral water

Regrowth in mineral water during 48 h of dark storage posterior to the irradiation experiment was observed only for the systems in the absence of H_2O_2 ($Fe^{2+}/h\nu$, $Fe^{3+}/h\nu$ and $h\nu$ only, Fig. 4). Subsequent total inactivation was maintained or completed posterior to 180 min irradiation during dark storage for the

Table 2
Summary of estimated observed inactivation rates (k_{obs} [min^{-1}]). Raw data was fitted in Matlab by the method of least squares which was weighted by the standard deviation for minimal triplicate measurement. The curves were either approximated by a one-term exponential ($N_t = N_0 e^{-k_{obs}t}$), leading directly to k_{obs} or by two different fittings, when shoulders were observed. In this case, k_{obs} was obtained by calculating a time weighted mean. The confidence interval for the fitting was 95% and deviation did generally not exceed 15%. For straight forward comparison, the variation of k_{obs} compared to $k_{obs}^{h\nu}$ which was set to 100% are displayed in brackets. $h\nu$ corresponds to simulated solar radiation (>290 nm). Temperatures did not exceed 38 °C.

Suspension matrix	Additives					
	$Fe^{2+}/H_2O_2/h\nu$ (**I**)	$Fe^{2+}/h\nu$ (**II**)	$Fe^{3+}/H_2O_2/h\nu$ (**III**)	$Fe^{3+}/h\nu$ (**IV**)	$H_2O_2/h\nu$ (**V**)	$h\nu$ only (**VI**)
MiliQ	0.15 ± 0.011	0.12 ± 0.003	0.146 ± 0.015	0.081 ± 0.008	0.088 ± 0.007	0.06 ± 0.009
(% compared to $h\nu$ only)	(250%)	(200%)	(145%)	(135%)	(150%)	(100%)
Mineral water	0.058 ± 0.008	0.042 ± 0.002	0.073 ± 0.007	0.033 ± 0.007	0.04 ± 0.002	0.048 ± 0.007
(% compared to $h\nu$ only)	(120%)	(90%)	(150%)	(67%)	(85%)	(100%)
Resorcinol [a]	0.19 ± 0.002	0.1 ± 0.009	0.212 ± 0.006	0.079 ± 0.006	0.122 ± 0.01	0.06 ± 0.009
(% compared to $h\nu$ only)	(320%)	(165%)	(355%)	(130%)	(200%)	(100%)
Saline [b]	0.16 ± 0.011	0.101 ± 0.004	–	–	0.088 ± 0.002	0.061 ± 0.004
(% compared to $h\nu$ only)	(260%)	(165%)			(145%)	(100%)
Saline dark	0.009 ± 0.002	0.017 ± 0.008	–	–	0.004 ± 0.002	0.001 ± 0.001
Trypton [c]	0.115 ± 0.013	0.113 ± 0.002	–	–	0.07 ± 0.008	0.032 ± 0.004
(% compared to $h\nu$ only)	(360%)	(350%)			(220%)	(100%)
Trypton dark	0.009 ± 0.007	0.02 ± 0.003	–	–	0.006 ± 0.005	0 ± 0.005

[a] 30 mg L^{-1}.
[b] 0.8 mg NaCl L^{-1}, 0.08 mg KCl L^{-1}.
[c] 0.1 g Trypton L^{-1}

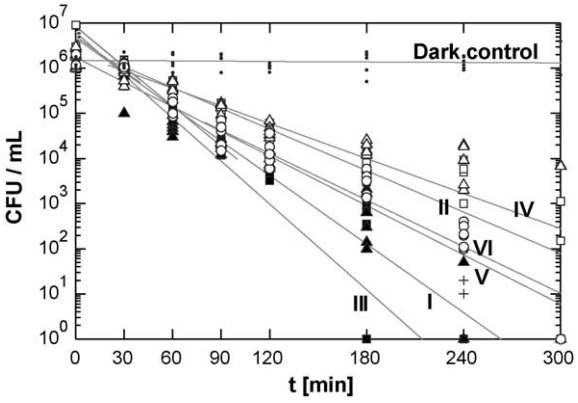

Fig. 3. Fenton-assisted photo-inactivation ($h\nu > 290$ nm) of *E. coli* suspended in mineral water (pH 7–7.5). Bacterial cells were harvested from stationary phase, washed and resuspended in the reactors. After acclimation, $Fe^{2+\text{ or }3+}$ and H_2O_2 were added to the corresponding systems. Remaining H_2O_2 was eliminated with catalase before plating. Markers represent raw data and lines show the resulting curve of a one-order exponential fitting. Calculated observed inactivation rates are displayed in Table 2. (**I**) (■) – 0.6 mg Fe^{2+} L^{-1}, 10 mg H_2O_2 L^{-1}; (**II**) (□) – 0.6 mg Fe^{2+} L^{-1}; (**III**) (▲) – 0.6 mg Fe^{3+} L^{-1}, 10 mg H_2O_2 L^{-1}; (**IV**) (△) – 0.6 mg Fe^{3+} L^{-1}; (**VI**) (+) – 10 mg H_2O_2 L^{-1}; (**V**) (○) – *hν* only; (**VII**) (·) – dark control (*E. coli* only). Dissolved iron ($Fe^{2+\text{ or }3+}$, after filtration) were measured simultaneously and were always lower than 0.2 mg L^{-1}.

systems $Fe^{2+}/H_2O_2/h\nu$, $Fe^{3+}/H_2O_2/h\nu$ and $H_2O_2/h\nu$. Note that when residual H_2O_2 was eliminated with catalase before dark storage, regrowth was observed for the system $Fe^{3+}/H_2O_2/h\nu$, but not for $Fe^{2+}/H_2O_2/h\nu$.

3.4. Inactivation in the presence of model organic matter

Fits on raw data are displayed in Fig. 5 and Table 2. The ranking for k_{obs} was: $Fe^{3+}/H_2O_2/h$ v > $Fe^{2+}/H_2O_2/h\nu$ > Fe^{2+}/h v > $H_2O_2/h\nu$ > $Fe^{3+}/h\nu$ > $h\nu$ only. Under $h\nu$ only, the presence of resorcinol did not affect the photo-inactivation compared to MilliQ. In the dark as well, resorcinol did not affect the bacterial population (Fig. 5, dark control, dark control resorcinol). In the systems Fe^{2+}/h v and $Fe^{3+}/h\nu$, photo-inactivation rates were enhanced up to 165, respectively 130% compared to the system $h\nu$ only (curve **II**, **IV** and **VI** in Fig. 5). The photo-inactivation in system $H_2O_2/h\nu$ was approximately 200% of $k_{obs}^{h\nu}$. This was probably due to H_2O_2 concentrations, which were increased up to 40 mg L^{-1} (against 10 mg L^{-1} in MilliQ and mineral water) in order to prevent scavenging by dissolved organic compounds. The higher H_2O_2 concentrations probably also contribute to the high inactivation rates. Photo-Fenton systems ($Fe^{2+}/H_2O_2/h\nu$ and $Fe^{3+}/H_2O_2/h\nu$) exhibit degradation rates values of 310 respectively 355% of $k_{obs}^{h\nu}$. Yet, synergistic factors were both still above 1 ($S_{Fe^{2+}/H_2O_2/h\nu} = 1.17$, $S_{Fe^{3+}/H_2O_2/h\nu} = 1.15$).

The photo-Fenton systems were also the most efficient for total organic carbon abatement ($Fe^{2+}/H_2O_2/h\nu$ and $Fe^{3+}/H_2O_2/h\nu$) and a TOC decrease of 90% was simultaneously observed along bacterial inactivation (Fig. 6).

Dissolved iron in the filtered samples was generally higher than in the absence of resorcinol (Fig. 7). Systems $Fe^{2+}/H_2O_2/h\nu$, $Fe^{2+}/h\nu$ and $Fe^{3+}/H_2O_2/h\nu$ showed a maximal concentration of approximately 0.5 mg L^{-1} after 1 h, whereas in system $Fe^{3+}/h\nu$, where Fe^{3+} was predominant over Fe^{2+}, iron concentration increased slightly over the total experimental period up to 0.4 mg L^{-1}.

3.5. Analysis of iron in the different suspension compartments

During the photo-inactivation experiment iron was measurable after filtration in the samples were Fe^{2+} was added. Whenever Fe^{3+}

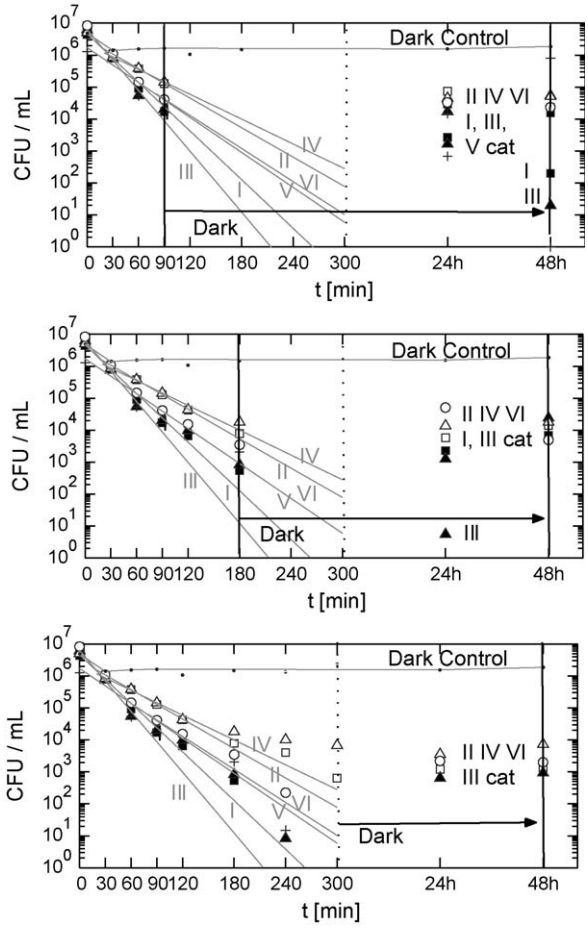

Fig. 4. Fenton-assisted photo-inactivation and post-irradiation events of *E. coli* suspended in mineral water (pH 7–7.5). Samples were taken after 90, 180 and 300 min of irradiation (*h* v) and placed in the dark for 24, respectively 48 h before remaining H_2O_2 was inactivated and subsamples manually plated. The results specified with *cat* describe samples were H_2O_2 was inactivated already with catalase before the dark storage period. Lines show the first-order fitting over the experimental period of 5 h under radiation which served for the calculation of k_{obs} (Table 2). Markers represent the average of raw data during irradiation and after 24 and 48 h when radiation was stopped after 90 min (top), 180 min (middle) 300 min (5 h, bottom). Where values where below the detection limit, these are not displayed. (**I**) (■) – 0.6 mg Fe^{2+} L^{-1}, 10 mg H_2O_2 L^{-1}; (**II**) (□) – 0.6 mg Fe^{2+} L^{-1}; (**III**) (▲) – 0.6 mg Fe^{3+} L^{-1}, 10 mg H_2O_2 L^{-1}; (**IV**) (△) – 0.6 mg Fe^{3+} L^{-1}; (**VI**) (+) – 10 mg H_2O_2 L^{-1}; (**V**) (○) – *hν* only; (**VII**) (·) – dark control (*E. coli* only).

or $Fe^{2+\text{ or }3+}/H_2O_2$ was added iron was not detected after filtration by the used method and no correlation of $Fe^{2+\text{ or }3+}$ concentrations in solution and bacterial inactivation was found. We therefore consider that Fe^{3+}, due to its higher charge density, was associated with the bacterial pellet and retained by the filter together with bacteria before measurement. In contrast, Fe^{2+} could be measured even after filtrations and elimination of the bacterial phase. To confirm this, we separated the different compartments of the experimental systems and measured iron concentrations in each of the three compartments. Table 4 recapitulates the results of total iron in the suspensions, iron in the bacterial pellet and iron in the solution (supernate after centrifugation) in the presence of MilliQ water only, saline solution (NaCl/KCl) or model organic matter (trypton or resorcinol).

For system $Fe^{2+}/H_2O_2/h\nu$ (**I**), when bacteria were prepared with saline solution or MilliQ water and then suspended in the reactors, 90–95% of total iron was associated with the bacterial pellet, whereas it was only 25% to 35%, when bacteria were prepared with resorcinol or trypton, an organic nutrient broth. When no H_2O_2 was added ($Fe^{2+}/h\nu$, **II**), only 40% of total Fe^{2+} were accumulated in the

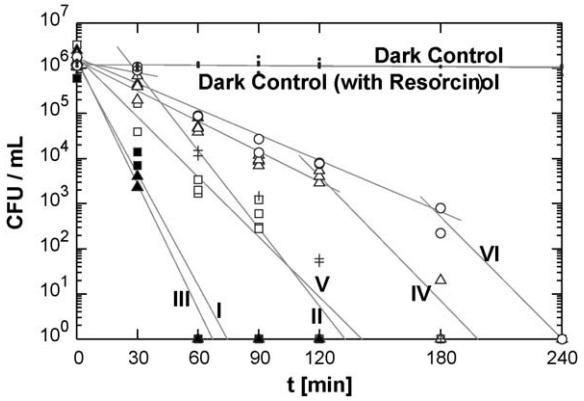

Fig. 5. Fenton-assisted photo-inactivation ($h\nu > 290$ nm) of *E. coli* suspended in MiliQ water (pH 5–5.5) containing 30 mg L^{-1} of resorcinol (19.6 ppm TOC). Bacterial cells were harvested from stationary phase, washed three times and resuspended in the reactors. After acclimation, $Fe^{2+\text{ or }3+}$, H_2O_2 and resorcinol were added to the corresponding systems. Initial H_2O_2 was 40 mg L^{-1} and remaining was always eliminated before plating. Markers represent raw data and lines show a one-order exponential fitting. Corresponding observed inactivation rates are displayed in Table 2. TOC and dissolved iron after filtration ($Fe^{2+\text{ or }3+}$) are shown in Figs. 6 and 7. (**I**) (■) – 0.6 mg Fe^{2+} L^{-1}, 40 mg H_2O_2 L^{-1}; (**II**) (□) – 0.6 mg $Fe^{2+}L^{-1}$; (**III**) (▲) – 0.6 mg Fe^{3+} L^{-1}, 40 mg H_2O_2 L^{-1}; (**IV**) (△) – 0.6 mg Fe^{3+} L^{-1}; (**V**) (+) – 40 mg H_2O_2 L^{-1}; (**VI**) (○) – $h\nu$ light; (**VIII**); (·) – dark control (*E. coli* and resorcinol only); (**IX**) (·) – dark control (*E. coli* only, no resorcinol).

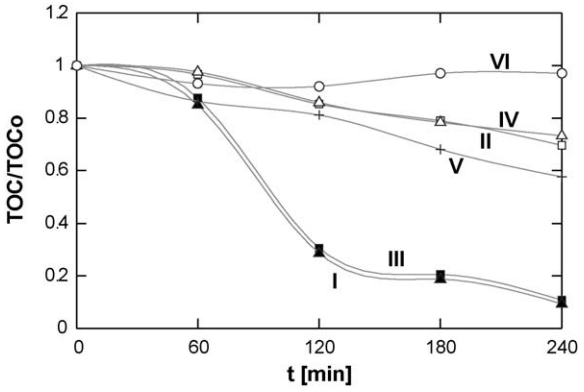

Fig. 6. Evolution of Total Organic Carbon (TOC) during photo-inactivation of *E. coli* suspended in MiliQ water containing 30 mg L^{-1} of resorcinol. Lines represent a polynomial multispline fitting over the average data points (markers). Corresponding bacterial inactivation curves and dissolved iron are shown in Figs. 5 and 7: (**I**) (■) – 0.6 mg Fe^{2+} L^{-1}, 40 mg H_2O_2 L^{-1}; (**II**) (□) – 0.6 mg $Fe^{2+}L^{-1}$; (**III**) (▲) – 0.6 mg Fe^{3+} L^{-1}, 40 mg H_2O_2 L^{-1}; (**IV**) (△) – 0.6 mg Fe^{3+} L^{-1}; (**V**) (+) – 40 mg H_2O_2 L^{-1}; (**VI**) (○) – $h\nu$ light.

bacterial pellet prepared with pure water and 20%, when bacteria were prepared with trypton.

For system $Fe^{3+}/H_2O_2/h\nu$ (**III**), 45% of total Fe^{3+} was found to be associated with bacteria prepared in pure water and the absence of H_2O_2 ($Fe^{3+}/h\nu$, **IV**) did not significantly change this result.

4. Discussion

4.1. E. coli suspended in MilliQ water

4.1.1. Photo-inactivation in MilliQ water in the presence of hv only (system VI)

Raw data and first-order fits of the observed photo-inactivation in MilliQ water (pH 5–5.5) are displayed in Fig. 2. The corresponding inactivation rates (k_{obs}) are presented in Table 2 (**VI**). Thermal inactivation can be excluded as temperatures did never exceed 38 °C [2,5]. Direct DNA damage by UVB can be

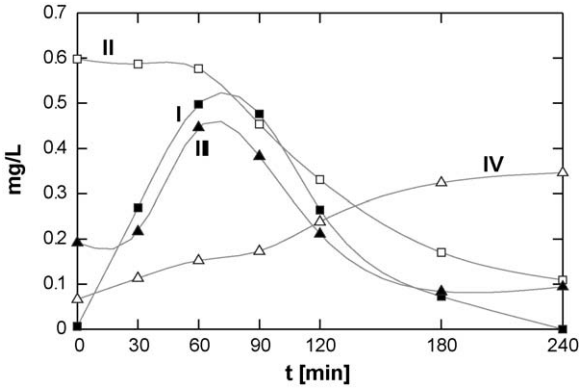

Fig. 7. Evolution of dissolved iron after filtration ($Fe^{2+\text{ or }3+}$) during photo-inactivation of *E. coli* suspended in MiliQ water (pH 5–5.5) containing 30 mg L^{-1} of resorcinol. Lines represent a polynomial multispline fitting over the average data points (markers). Corresponding bacterial inactivation curves are shown in Fig. 5: (**I**) (■) – 0.6 mg Fe^{2+} L^{-1}, 40 mg H_2O_2 L^{-1}; (**II**) (□) – 0.6 mg $Fe^{2+}L^{-1}$; (**III**) (▲) – 0.6 mg Fe^{3+} L^{-1}, 40 mg H_2O_2 L^{-1}; (**IV**) (△) – 0.6 mg Fe^{3+} L^{-1}.

excluded as the used solar simulator emits negligible amounts of photons at wavelength shorter than 300 nm. In MilliQ water, exogenous photosensitization is not expected. The observed photo-inactivation is probably due to excitation of endogenous photosensitizers, such as cytochrome, flavin, tryptophan and other aromatic amino acids [3,6], attack of cellular constituents by ROS and DNA damage by •OH [29,50]. An excited endogenous photosensitizer may react directly with cellular biomolecules (type I reactions), or more commonly, with surrounding O_2 (type II) leading to the generation of ROS such as $^1O2$, $O_2^{\bullet -}$, •OH and H_2O_2. Type I reactions include the attack of proteins and cell membrane components, especially membrane lipids [51], leading to lipid peroxidation chains [52] and the inactivation of the cells (e.g. because of increased permeability and/or the disruption of trans-membrane ion gradients) [4]. ROS generated via type II reactions can also monitor these attacks. H_2O_2 can additionally react with intracellular free or loosely bound ferrous iron (or another divalent metal ion) to form highly reactive •OH another toxic oxygen species via the Haber–Weiss (Eq. (1)) reaction (intracellular Fenton) [50].

In general, the reduced forms of these metal ions produce •OH at a faster rate upon reaction with H_2O_2 than the oxidized forms. Therefore, reducing agents such as $O_2^{\bullet -}$, $FADH_2$ or NAD(P)H, which catalyze the regeneration of Fe^{2+} from Fe^{3+}, can accelerate the generation of •OH [53,26,52,50,28]:

$$Fe^{3+} + Donor^{red} \rightarrow Fe^{2+} + Donor^{ox} \quad (8)$$

•OH reacts at, or close to, a diffusion-controlled rate. Hence any formed •OH will react with whatever is present at its formation site and directly damage almost all biological molecules, including DNA [54]. Until today, no cellular defense mechanism against the attack of DNA by •OH has been identified and these radicals, once generated inside the cells, are therefore extremely toxic [55].

When the concentration of active oxygen species (or ROS) increases to a level that exceeds the cell's defense capacity, this is called oxidative stress [52]. Because the cellular defense system against oxidative stress (e.g. catalase) are also known to be light-sensitive, photo-inactivation is simultaneously initiated by two ways: (i) photosensitization increases the intracellular presence of ROS leading to direct attack of membrane and other proteins; (ii) the photo-degradation of catalase, which in normal conditions would continuously eliminate exceeding intracellular H_2O_2, allows the generation of highly reactive •OH via intracellular Fenton reactions, leading to direct DNA damage.

The oxygen dependent ROS formation and following membrane lipid peroxidation and DNA damage is nowadays perceived as the major components of photo-inactivation in the SODIS process [56,4].

4.1.2. Photo-inactivation in the presence of H_2O_2 in MilliQ water (Fig. 2 and Table 2, system V)

The photo-inactivation rate in the presence of H_2O_2 was enhanced by 50%. We identified three possible pathways, which could be at the origin of this enhanced inactivation: First, $H_2O_2/h\nu$ is a photo-assisted advanced oxidation process commonly used for the degradation of chemical pollutants via the photolysis of H_2O_2 and the subsequent formation $^{\bullet}OH$ [57]. However, H_2O_2 absorbs photons only meaningfully at wavelength below 250 nm, the quantum yield is generally low and the backside of the high reactivity of $^{\bullet}OH$ is its extremely short lifetime, limiting its mobility in any system. Therefore, this pathway probably plays an minor role during observed bacterial inactivation. Secondly, H_2O_2 or derived oxygen species can directly attack the cellular membrane, initiating lipid peroxidation chains that increase membrane permeability and affect the viability of the cells [53]. This pathway probably plays a role, but the experimental results do not allow a quantification of its contribution to overall inactivation. Third, H_2O_2 is relatively stable (unlike $^{\bullet}OH$) and uncharged (unlike $O_2^{\bullet-}$), and therefore penetrates membranes and diffuse into cells whenever H_2O_2 is present in the extracellular habitat [29]. An overload of intracellular H_2O_2 increases the possibility of $^{\bullet}OH$ generation via Fenton reaction with intracellular free or loosely bound iron as discussed in the previous paragraph. If iron ions are not available, H_2O_2 can cause the oxidation of iron sulfur clusters ([4Fe-4S]) and the release of Fe^{3+}, which if reduced to Fe^{2+}, contributes to intracellular Fenton reactions [50]. Additionally, Fe^{2+} can be directly liberated when UVA (320–400 nm) damages some iron containing proteins such as enterobactin [58] or ferritin [59]. Moreover, $O_2^{\bullet-}$, a byproduct of aerobic respiration (auto-oxidation of $FADH_2$) [50] or generated by endogenous photosensitization [3,6], can oxidize [4Fe-4S] causing the release of Fe^{2+} and the simultaneous generation of additional H_2O_2 [60,8,50]. The generated transient iron overload, produces strongly favorable conditions for the production of highly reactive $^{\bullet}OH$ and other toxic oxygen species in the presence of H_2O_2 via the Haber–Weiss reaction (Eq. (1)) [58]58]. But, because of its short life-time, the localization of the production site of $^{\bullet}OH$ is determining for the localization and nature of caused damage. Consequently large portion of H_2O_2 dependent DNA damage appears due to Fenton reactions directly on Fe^{2+} associated with DNA [61].

In the absence of light, we did not observe a bactericidal effect of H_2O_2 and the effect of H_2O_2 and light seems to be synergistic [6]. The synergy arises from the ability of UVA radiation to damage the enzyme catalase, which is important for the cellular defense against oxidative stress [62,29]. As mentioned above, catalase scavenges intracellular H_2O_2 and controls its concentration via the following reaction:

$$H_2O_2 + H_2O_2 \xrightarrow{cat} 2H_2O + 2O_2 \quad (9)$$

When catalase is damaged, intracellular H_2O_2 increases to toxic concentrations especially in the presence of extracellular H_2O_2, which diffuses inside the cells.

Superoxide dismutase (SOD) is another enzyme involved in the cellular defense against oxidative stress. SOD is able to scavenge $O_2^{\bullet-}$, transforms it into H_2O_2 and thus contributes to enhanced H_2O_2 concentrations:

$$O_2^{\bullet-} + O_2^{\bullet-} + 2H^+ \xrightarrow{SOD} H_2O_2 + O \quad (10)$$

SOD might also be inactivated by UVA as many other enzymes [63]. That might seem at first sight to be beneficial for the bacteria because the generation of H_2O_2 would be precluded. However, $O_2^{\bullet-}$ plays an important role in intracellular Fenton reactions, because an overload can also be induced by radiation (i.e. photosensitization), $O_2^{\bullet-}$ is responsible for the oxidation of [4Fe-4S] cluster present in cells, the subsequent release of Fe^{2+} and the simultaneous formation of H_2O_2 and itself can also serve as a reducing agent for the regeneration of Fe^{2+} from Fe^{3+}[64,60,8,50]. The sum of the effect of light on the cellular antioxidants system and the intracellular overload of H_2O_2 and iron, constitutes a catalytic system leading to considerably enhanced photo-inactivation.

The synergistic bactericidal effect of H_2O_2 and light has been reported previously [6,29,65]. However, for a real scale application, the availability of H_2O_2 in developing countries has to be assessed. Further up to know little is known about long term health concern of H_2O_2 for human consumption and therefore, residual H_2O_2 should be avoided.

4.1.3. Photo-inactivation in the presence of Fe^{2+} or Fe^{3+} in MilliQ water (Fig. 2 and Table 2, systems II and IV)

For $Fe^{2+}/h\nu$ we did observe an enhancement of 100% of the reference bacterial inactivation rate ($k_{obs}^{h\nu}$) while it was only 35% in the presence of $Fe^{3+}/h\nu$. The bactericidal effect of Fe^{2+} probably arises from its ability to diffuse into the cells, leading to the generation of $^{\bullet}OH$ via intracellular Fenton reactions when reacting with metabolic H_2O_2 [66,29,50]. This effect can also be observed in nature: In well waters, for instance, which contain little oxygen and therefore stable Fe^{2+}, bacteria such as *E. coli* and *S. typhimurium* are rapidly killed by taking up excessive concentrations of ferrous iron [67].

The effect of the simultaneous presence of Fe^{2+} and light in MilliQ water, compared to the lower effect of Fe^{2+} in the dark (Table 2, MilliQ and Saline Dark, system **II**) let us suggest a synergistic interaction of Fe^{2+} and $h\nu$. This synergy would arise, on one hand from the ability of Fe^{2+} to easily diffuse into the cells [68] and on the other hand, from the catalase inactivation by UVA radiation. In consequence, in the presence of light, enhanced intracellular Fe^{2+} concentrations may increase the intracellular Fenton reactions and consequently enhanced the generation of $^{\bullet}OH$. Because some H_2O_2 is always produced during cellular metabolic activity (e.g. catalyzed by enzymatic activity [52,29]), Fe^{2+} can also provoke this damage in the dark as it was observed (Table 2, Saline Dark, **II**).

The diffusion of Fe^{2+} inside the cells is most probably due to its lower charge density compared to Fe^{3+} and increased by osmotic stress. We did not measure dark inactivation rates in the presence of Fe^{3+}. But Fe^{3+} is expected not to influence the growth or viability of *E. coli* in the dark. In contrast, Fe^{3+} can serve as an electron acceptor instead of oxygen in facultative anaerobic respiration of *E. coli*, while only some acidophylic chemolithotrophs (i.e. *Thibacillus ferrooxidans* or *Leptospirillum ferrooxidans*) can use Fe^{2+} for respiration and growth. Further, the insolubility of Fe^{3+} at higher pH precludes its mobility as a metal ion for microorganism. To manage transport of Fe^{3+} into the cell, *E. coli* K12 has several highly specific outer membrane binding proteins to transfer iron into the cytoplasm. Once in the cytoplasm, siderophores, specifically designed to chelate Fe^{3+} selectively (e.g. hydroxamates, catecholates, carboxylates or heterocyclic compounds) overtake Fe^{3+} and deliver it inside the cell [68]. Because Fe^{3+} cannot move freely into the cells, once inside the cell, the reaction with H_2O_2 is considerably less rapid, and as Fe^{3+} can be used for facultative respiration by *E. coli*, it is intuitively understandable that the bactericidal effect of Fe^{3+} is less pronounced than for Fe^{2+}.

However, the observed inactivation rate for $Fe^{3+}/h\nu$ in MilliQ under irradiation was still 35% higher than for the system with only *hν*. We suggest that in our conditions, Fe^{3+} adsorbs on bacteria instead of diffusing inside the cells, leading to the formation of Fe^{3+}-bacteria exciplexes. Indeed, for the degradation of organic pollutants, it has been established that carboxylates, polycarboxylates or aminopolycarboxylic acids form strong photo-active complexes (exciplexes) with Fe^{3+}[69,70,27] and that the photo-degradation of these organic molecules is sensitized by Fe^{3+}[34]. It was also observed that the Fenton reaction seems to be independent of molecular weight and that the degradation can take place within aggregates of macro-molecules and Fe^{3+}[28]. Such complexes might also be formed by bacteria, as supra-macro-biomolecules and Fe^{3+}. In Fe^{3+}-organo complexes with polycarboxylates, the excitation of the Fe^{3+} chelate into a LMCT state by light can be followed by photo-induced electron transfer, leading to reduction of Fe^{3+} to Fe^{2+} and oxidation of the chelating ligand. If the ligand radical generated reacts with O_2, a sequence of oxidants ($O_2^{\bullet-}$, $^{\bullet}OH$, H_2O_2) is produced [34] similar to that observed during photosensitization. The generated Fe^{2+} can than directly react with H_2O_2 via the Haber–Weiss (Eq. (1)), leading to additional $^{\bullet}OH$ and the concomitant formation of Fe^{3+}.

But in the absence of H_2O_2, Fe^{2+} is also effectively oxidized by O_2, either in a single step photo-reaction with the formation of $O_2^{\bullet-}$ [71], via the reaction of Fe^{2+} with $^{\bullet}OH$ or HO_2[72], or both combined with the subsequent formation of H_2O_2 [73,74]. In the atmosphere, for instance, the photo-oxidation of Fe^{3+}-oxalate and the depletion of oxalic acid has been identified as the predominant source of H_2O_2 and $^{\bullet}OH$ [70].

Bacterial cell walls possess highly reactive surfaces able to bind iron and impact the cycling of iron in natural aquatic systems [75]. The membrane of the Gram negative bacteria *E. coli* consists of a cytoplasm a periplasm and an outer membrane. Besides the siderophores produced in the cytoplasm and the iron binding proteins in the outer membrane, other proteins of the bacterial membrane and their carboxylic endgroups are likely to show an affinity for Fe^{3+} and to support the formation of Fe^{3+}-bacteria bounds. The formation of Fe^{3+}-bacteria complexes are therefore probably at the origin of the higher observed inactivation rates in the presence of Fe^{3+}. If these complexes would be photo-active, they would contribute to the bacterial inactivation on one hand via direct oxidation of the membrane constituents and on the other via the generation of Fe^{2+}, H_2O_2 and $^{\bullet}OH$ within spitting distance of the target bacteria [71–74].

The role of iron in lipid peroxidation chains in living organisms has been reported previously [64,26]. However, photo-Fenton systems do considerably take advantage of light because of the photoactivity of some Fe^{3+}-hydroxy complexes, which allow the fast (re-)generation of Fe^{2+} and generation of ROS in the bulk. But the most photo-active of Fe^{3+}-hydroxy ($FeOH^{2+}$) is predominant at pH ≈ 2.8 [33,27,28] and the photo-activity of $FeOH_2^+$, which is the predominant species at higher pH, has not been quantified and appears to be much lower [34].

Table 3
Summary of calculated synergistic factors ($S_{Fe/H_2O_2/h\nu} = (k_{obs}^{Fe/H_2O_2/h\nu}/k_{obs}^{(Fe+H_2O_2)/h\nu})$).

Suspension matrix	Synergistic factors		
	$S_{Fe^{2+}/H_2O_2/h\nu}$ (**I**)	$S_{Fe^{2+}/H_2O_2/dark}$ (**II**)	$S_{Fe^{3+}/H_2O_2/h\nu}$ (**III**)
MiliQ	1.01	–	1.4
Mineral water	1.7	–	2.92
Resorcinol	1.17	–	1.15
Saline NaCl/KCl	1.25	0.45	–
Trypton	0.84	0.38	–

As mentioned, the toxicity of Fe^{2+} for *E. coli* due to intracellular generation of $^{\bullet}OH$ has been already detected but is not studied in detail. But due to the rapid oxidation of Fe^{2+} to Fe^{3+} in natural oxygenated water, the importance of Fe^{2+} is reduced for solar water disinfection. However, the observation that Fe^{3+} under simulated solar light in the presence of oxygen increases the photo-inactivation rates is for real situation of relevance, because ferric iron is available as a low-cost additive and often naturally present in drinking water sources.

4.1.4. Photo-inactivation in the presence of $Fe^{2+\ or\ 3+}$ and H_2O_2 in MilliQ water (Fig. 2 and Table 2, systems I and III)

In the presence of the classical photo-Fenton system ($Fe^{2+\ or\ 3+}/H_2O_2/h\nu$), we observed the highest inactivation rates for *E. coli* suspended in MilliQ. In these systems, the above cited processes leading to $^{\bullet}OH$ and ROS generation inside or close to the cells may occur simultaneously. Additionally, the presence of extracellular H_2O_2 may increase the permeability of the bacterial membrane for Fe^{2+} diffusion and the roughness for Fe^{3+} attachment.

Moreover, Fenton (Fe^{2+} and H_2O_2) and photo-Fenton (i.e. photolysis of Fe^{3+}-hydroxo complexes) in the bulk could generate extracellular $^{\bullet}OH$ and ROS, attacking the bacterial cells from the outside, initiating lipid peroxidation chains and leading to enhanced membrane permeability.

To better understand the contribution of each isolated system in bacterial photo-inactivation (Fe^{2+}, Fe^{3+} or *hν*) and their respective interaction with H_2O_2, synergistic factors (*S*) for the simultaneous presence of $Fe^{2+\ or\ 3+}$ and H_2O_2 were calculated (Table 3).

$S_{Fe^{2+}/H_2O_2/h\nu} \approx 1$ in MilliQ water indicates that in the simultaneous presence of both, Fe^{2+} and H_2O_2 does not induce a enhanced bacterial inactivation compared to the sum of the bactericidal effect of $Fe^{2+}/h\nu$ and $H_2O_2/h\nu$ systems. According to the suggestion, that the presence of Fe^{2+} alone in the presence of *hν* leads to bactericidal conditions due to intracellular dark Fenton reaction, it is proposed, that effect of the additional ROS generation in the $Fe^{2+}/H_2O_2/h\nu$ system is masked by the lower effect of Fe^{2+} alone due to rapid transformation to Fe^{3+} in the presence of H_2O_2.

In contrast, the simultaneous presence or Fe^{3+} and H_2O_2 leads to a synergistic inactivation ($S_{Fe^{3+}/H_2O_2/h\nu} \approx 1.4$). This synergistic action could arise from photo-Fenton and Fenton reactions on Fe^{3+}-bacteria bounds as described above and which are enhanced in the presence of H_2O_2 because of increased production of $^{\bullet}OH$ and faster Fe^{2+}/Fe^{3+} interconversion.

For the classical degradation of chemical pollutants by Fenton systems ($Fe^{2+\ or\ 3+}/h\nu$), it is, from a mechanistic point of view, meaningless to distinguish ferrous from ferric type iron reactions, due to the fast oxidation of Fe^{2+} to Fe^{3+} in the presence of H_2O_2[28]. In contrast, for photo-Fenton like reactions the distinction is significant, because of dissimilarities in the affinity for the formation of photoactive complexes. For biological systems (i.e. *E. coli* bacteria) the differentiation is also relevant because of differentiated ways of action for each species: Fe^{3+} has a higher probability to adsorb on cells and to form exciplexes on the bacterial membrane because it can not easily diffuse into the cells and can bind on specific proteins; Fe^{2+} can diffuse into cells, especially in the presence of osmotic forces.

Further evidence that Fe^{3+} has an affinity to associate with bacteria, were also given by the measurement of dissolved iron. No iron could be detected in the solutions after separating the bacterial phase by filtration in the systems containing Fe^{3+} ($Fe^{3+}/h\nu$, $Fe^{3+}/H_2O_2/h\nu$ and $Fe^{2+}/H_2O_2/h\nu$). In contrast, for the system $Fe^{2+}/h\nu$, Fe^{2+} was detected.

Another evidence for the significance of the oxidation state of iron in microbiological systems is given by the fact that in system Fe^{2+}/dark, bacterial inactivation was observed to a much higher

degree than in the system Fe^{2+}/H_2O_2/dark, where Fe^{2+} is rapidly oxidized to Fe^{3+}.

In MilliQ water, the overall effect on *E. coli* photo-inactivation was similar for the systems based on Fe^{2+} ($Fe^{2+}/H_2O_2/h\nu$) or Fe^{3+} ($Fe^{3+}/H_2O_2/h\nu$). However, the specific effect of Fe^{2+} and Fe^{3+} in the absence of H_2O_2, discussed in the previous paragraph, indicates that their mode of action are not the same. While Fe^{2+} might diffuse into the cells and cause the production of •OH inside the cells, Fe^{3+} binds to the cellular membrane and thus generates localized ROS by photo-Fenton reactions.

The identification of these specific reaction modes is relevant, because iron is generally present as Fe^{3+} in natural water and represents a low-cost photocatalyst for solar water disinfection. Moreover, H_2O_2 would probably be the most effective electron donor (and acceptor) for driving solar photo-Fenton disinfection in real scale applications.

4.2. E. coli suspended in mineral water

To simulate inorganic ions generally present in natural waters, we replaced the MilliQ in our experimental system by commercial mineral water containing a complex mixture of HCO_3^-, Ca, SO_4^-, Na, Cl, Mg, $Si(OH)_4$, K and NO_3^- (Table 1). In this experimental series, pH was initially 7.5 and did remain above 7 during the entire period.

4.2.1. Photo-inactivation in the presence of hν only in mineral water (Fig. 3 and Table 2, system VI)

The presence of inorganic ions, compared to MiliQ water involves reduced stress for *E. coli* because less energy is required for maintaining osmotic pressure and ions necessary for the metabolic activity are highly abundant. k_{obs} for *E. coli* inactivation in mineral water is therefore lower.

The sensitivity of bacteria to photo-inactivation always depends on the nature of water. The inhibitory effect of inorganic ions on solar water disinfection has been observed earlier, in particular for Cl^- and SO_4^-, while NO_3^- and HCO_3^- had a beneficial effect [76,77,16], although a negative impact of carbonates had also been observed during the photo-catalytic bacterial inactivation [e.g. 78]. However, because of the complex nature of applied inorganic ions mixture, we did not dissociate the impact of each specific ionic component. One part of the observed bactericidal effect of light ($h\nu$), is probably caused by the same mechanisms as observed in MilliQ water and discussed above. Additionally, the irradiation of the systems might also involve the formation of inorganic radicals like bicarbonate radicals that can affect the integrity of the bacterial membrane [76].

4.2.2. Photo-inactivation in the presence of H_2O_2 in mineral water (Fig. 3 and Table 2, system V)

The presence of H_2O_2 in mineral water, in contrast to the same system in MilliQ water (Fig. 2), did not increase bacterial photo-inactivation and k_{obs} for $H_2O_2/h\nu$ was 85% of the one for $h\nu$ only (the 15% difference lies within the standard deviation). The presence of inorganic ions does protect the *E. coli* from osmotic stress and might also inhibits excessive diffusion of H_2O_2 inside the cells. The inorganic ions may enter in competition with H_2O_2 for contact sites on the cellular membrane, protecting it from direct attack by H_2O_2 and other ROS. Gogniat et al. [79] for instance reported that the composition and nature of inorganic ions in aqueous *E. coli* suspensions considerably influences the adsorption of the bacteria onto the photocatalyst TiO_2 and therefore determines the photo-inactivation process. Besides, scavenging of bactericidal radicals by inorganic ions, as observed for the photo-catalytic inactivation of *E. coli* by Rincon [76] also plays a role in our case. Kochany and Lipczynska-Kochany [80] previously reported that carbonate, and bicarbonate anions quench the hydroxyl radicals in H_2O_2/h ν system.

4.2.3. Photo-inactivation in the presence of Fe^{2+} or Fe^{3+} in mineral water (Fig. 3 and Table 2, systems II and IV)

The systems $Fe^{2+}/h\nu$ and Fe^{3+}/h ν in mineral, in contrast to the same systems in MilliQ water (Fig. 2), did not show any enhancement of the bactericidal effect compared to the system $h\nu$ only. Indeed, inorganic ions do not only affect the sensitivity of bacteria and the availability of contact sites on the membrane surfaces, but also the speciation of iron, which is already less favorable for the solubility of Fe ions than in the MilliQ system because of the considerable higher pH (7–7.4).

The most fitting scenario might would be that pH significantly decreases the mobility of iron and that inorganic ions present in mineral water hinder the contact between the iron cations and bacteria, preventing both, Fe^{2+} diffusion into the cell and the formation of Fe^{3+}-bacteria exciplexes.

These results are somehow discouraging as natural raw drinking water generally contains a variety of inorganic and organic ions, and it is extremely difficult to predict the antagonistic or synergistic interactions of the various components in such systems. Thus, the experimental mineral water used for this study, contained rather high concentrations of ions, especially for HCO_3^-, which could quench •OH [80]. Further, in contrast to our study and the one of Kochany and Lipczynska-Kochany [80], it was also reported that HCO_3^- can enhance solar bacterial inactivation [77]. This observation illustrates the black-box problem often faced in the development of water treatment technologies as the efficiency of such treatment systems at real scale varies strongly with the changing chemical characteristics of drinking water sources.

4.2.4. Photo-inactivation in the simultaneous presence of $Fe^{2+\ or\ 3+}$ and H_2O_2 in mineral water (Fig. 3 and Table 2, systems I and III)

Fenton and photo-Fenton oxidations of organic compounds are inhibited in varying degrees by inorganic ions (e.g. phosphate, sulfate, chloride), depending on their concentrations and via precipitation of iron, scavenging of •OH or coordination to dissolved Fe^{3+} to form less reactive complexes [28].

Despite the high abundance of various inorganic ions, the absence of osmotic stress, a pH of 7–7.5 and the absence of a bactericidal effect of $H_2O_2/h\nu$ or $Fe^{2+\ or\ 3+}/h\nu$, both photo-Fenton systems ($Fe^{2+\ or\ 3+}/H_2O_2/h\nu$) resulted in a considerably higher k_{obs} than $h\nu$ only. Therefore, observed synergistic factors for the simultaneous presence of iron and H_2O_2 under irradiation were particularly high. Further, and in contrast to the experiment in MilliQ water, where the overall effect of the system based on Fe^{2+} and Fe^{3+} was similar, $Fe^{3+}/H_2O_2/h\nu$ resulted in a higher bacterial inactivation than $Fe^{2+}/H_2O_2/h\nu$ in mineral water. In consequence, one could conclude that ,among the pathways for bacterial photo-inactivation cited until now , ROS generation via classical photo-Fenton reactions in the bulk are at the origin of high synergistic effect of $Fe^{2+\ or\ 3+}/H_2O_2/h\nu$.

Admittedly, it is generally accepted that the photo-Fenton system is strongly limited by pH, because at near neutral pH, Fe^{3+} tends to precipitate and the predominant Fe-hydroxy species are less photoactive than species present at lower pH [33,27]. Further, •OH radicals have an extremely short lifetime, and must be produced near the bacterial membrane if they were to oxidize some of its components [79]. Regarding the high synergistic factors, it is therefore likely that observed bacterial inactivation, additionally to the conventional ROS formation in the bulk via photo-Fenton, were also supported by the diffusion of Fe^{2+} inside the cells, the deposition of Fe^{3+} on and the attack by H_2O_2 of the bacterial membrane as observed in MilliQ water, even though these photo-inactivation pathways were only significant when the

different reagents were present simultaneously. However, one must bear in mind the possibility of the involvement of other reactive species such as high-valent oxorion (ferryl) or inorganic radicals (e.g. bicarbonate radical) in addition to, or instead of, $^{\bullet}OH$ [38,28,24].

4.3. Post-irradiation effects in mineral water

Pour-plating does not allow to distinguish between inactivation and death and irradiation might only causes a sublethal damage: when previously irradiated cells are cultured aerobically, a burst of free radical production due to a light-induced aftereffect kills them retrospect, rather than the initially light-induced stress [81]. These sublethally damaged cells might not be aerobically culturable when directly plated after the irradiation period, but recover when kept in the dark [4]. Optical inactivation in SODIS systems is therefore sometimes reversible [9,82], because only a small amount of recovering and surviving cells would be sufficient for regrowth in the presence of easily assimilable organic carbon such as natural organic matter or lysate of dead cells.

To increase the accuracy of the here applied pour-plating method, we always added catalase before performing aerobic plating and incubations in order to eliminate residual H_2O_2[83]. Further we measured regrowth in samples, which have been stored for 24, respectively 48 h in the dark (Fig. 4).

4.3.1. Post-irradiation effects in mineral water in the presence of hν only and H_2O_2/h ν

Even though k_{obs} for the system with only *h* ν and H_2O_2/*hν* were not significantly different in mineral water (Table 2), no regrowth was observed in the presence of H_2O_2 when H_2O_2 was eliminated with catalase before dark storage, while in the presence of *hν* only, regrowth occurred even when complete inactivation was observed before dark storage (Fig. 4, **VI** and **V**). This result illustrates the long-term effect of H_2O_2 after initial illumination also in mineral water.

4.3.2. Post-irradiation effects in mineral water in the presence of Fe^{2+} or Fe^{3+}

In the presence of iron alone, complete bacterial inactivation was not achieved during the photo-treatment and the bacterial population remained stable during 48 h in the dark (Fig. 4, **II** and **IV**). These results are not surprising because in mineral water, over the experimental period of 4 h, no bactericidal effect of illuminated Fe^{2+} or Fe^{3+} was observed (Table 2) due to competition of inorganic ions for contact sites for within the bacterial membrane and $Fe^{2+\text{ or }3+}$.

4.3.3. Post-irradiation effects in mineral water in the presence of $Fe^{2+\text{ or }3+}$ and H_2O_2

In the simultaneous presence of $Fe^{2+\text{ or }3+}$ and H_2O_2 and when total inactivation was reached before dark storage, no regrowth was observed in the presence of residual H_2O_2 (>5 mg L^{-1} after 48 h, Fig. 4, **I** and **III**). Interestingly, when H_2O_2 was eliminated by the addition of catalase before dark storage, regrowth was observed for the system based on Fe^{3+} while in the presence of Fe^{2+} no bacteria were measured even after 48 h of dark storage (Fig. 4, **Icat** and **IIIcat**). This result indicates that residual H_2O_2 after irradiation has a residual effect and supports the affirmation that inactivation is presence of Fe^{3+} would be due only to photo-Fenton reactions on the bacterial surface and thus entirely depending on irradiation. In contrast, inactivation in the presence of Fe^{2+} and H_2O_2 results probably from a combination of intracellular dark Fenton as well as from classical photo-Fenton reactions.

Regarding this post-irradiation experiment, two observations seem highly interesting: First, in the presence of residual H_2O_2, regrowth was always absent. And second, when H_2O_2 was eliminated before dark storage, regrowth did only occur for the system $Fe^{3+}/H_2O_2/h\nu$ and not for $Fe^{2+}/H_2O_2/h\nu$. These results motivates our suggestion about the assessment of a low-cost availability of H_2O_2 for real scale drinking water treatment (e.g. electrochemical *in situ* generation). Further, for water treatment, were iron is not naturally present, it would probably be more interesting to add Fe^{2+}. The latter could also be generated *in situ* by the photo-dissolution of zerovalent iron as it has been done for the low-cost removal or arsenic from drinking water [43].

4.4. E. coli suspended in MilliQ water containing resorcinol as model organic matter (NOM)

4.4.1. Photo-inactivation with the systems hν and H_2O_2/hν in the presence of resorcinol (Fig. 5 and Table 2, systems VI and V)

The initial pH was 5.5 and did not decrease below 5 during the photo-treatment. When bacteria were exposed to *hν* only, the inactivation rates were similar in the presence and absence of resorcinol (compare with Fig. 2) and a dark control confirmed that resorcinol alone does not affect the *E. coli* population. The presence of H_2O_2 did enhance photo-inactivation by 100% compared to *hν* only. This effect was only 50% in MilliQ water (Table 2), but H_2O_2 concentrations were considerably higher than in the in MilliQ water experiment (40 mg L^{-1} vs. 10 mg L^{-1}). Resorcinol was mineralized by 40%.

4.4.2. Photo-inactivation in the presence of Fe^{2+} and Fe^{3+} and resorcinol (Fig. 5 and Table 2, systems II and IV)

The effects of both $Fe^{2+}/h\nu$ and $Fe^{3+}/h\nu$ (Fig. 5) were similar to those observed in the absence of resorcinol (Fig. 2) although k_{obs} for $Fe^{2+}/h\nu$ was slightly lower. Resorcinol might competes for Fe^{2+} and limits the contact to bacteria for intracellular diffusion. However, illuminated Fe^{2+} had still a higher bactericidal effect than Fe^{3+} and in the dark in the presence of trypton (an organic nutrient broth, Table 2), Fe^{2+} alone did also cause bacterial inactivation, while when both Fe^{2+} and H_2O_2, and thus Fe^{3+} was predominant over Fe^{2+}, this effect was less pronounced. Therefore the inactivation via intracellular Fenton in the presence of Fe^{2+} may take place.

Resorcinol might also enters in competition with bacteria to coordinate with Fe^{3+}, but this does not affect the overall efficiency of the system because the photo-active Fe^{3+}-resorcinol complexes (or Fe^{3+}-resorcinol by products) could replace and compensate the effect of Fe^{3+}-bacteria exciplexes. Further, the formation of bacteria-Fe^{3+}-resorcinol exciplexes and aggregates is likely because there is no competition with other components in MilliQ water media. We do not have explicit evidence for Fe^{2+} or Fe^{3+}-resorcinol exciplex formation. But it is generally accepted that carboxylates, a potential resorcinol degradation intermediate, do form photo-active complexes [28,36,69]. The photolysis of Fe^{3+} complexes with organic ligands, which have generally a high molar absorption coefficient in UVA and visible light leads to the regeneration of Fe^{2+} and the formation of a ligand radical [34]. The Fe^{3+}-(L) complex thereby undergoes LMCT:

$$Fe^{3+} - (L)_n + h\nu \rightarrow Fe^{2+} - (L)_{n-1} + L_{ox}^{\bullet} \quad (11)$$

Both, Fe^{2+} and radicals can react with O_2 leading to the formation of ROS ($O_2^{\bullet -}$, $^{\bullet}OH$, H_2O_2) [34], which may attack cellular membrane constituents and initiate membrane lipid peroxidation, enhancing the permeability and roughness of the membrane [52,69,51,53]. In a second step, Fe^{2+} directly reacts with H_2O_2 via the Haber–Weiss reaction (Eq. (1)), leading to the regeneration of Fe^{3+} and the production of $^{\bullet}OH$. Because at pH above 3, Fe^{3+} tends to precipitate, Fe^{3+}-organo complexes play an important role for the efficiency of photo-Fenton systems at near neutral pH [36,37,22,24]. If the so formed ROS occur close to the bacterial

surfaces, they lead to external cell damage. Moreover, the *in situ* formed H_2O_2 can lead to intracellular dark Fenton reactions as discussed before. The generated organic radicals (L_{ox}) might also attack bacterial cell membranes, but they are subsequently oxidized and after a certain reaction time loose their ability to form iron chelate [36].

Dissolved iron measured in the filtered samples (Fig. 7) is generally higher than in the absence of resorcinol supporting the assumption that resorcinol and its degradation intermediates do have a chelating effect favoring the maintenance of $Fe^{2+\text{ or }3+}$ in solution. TOC is not significantly affected during the experiment (Fig. 6, **II** and **IV**), but this does only mean that resorcinol is attacked and transformed into other organics, which might be even more suitable for iron chelation than resorcinol itself.

These results indicate again that the iron-catalyzed photo-inactivation systems are highly sensitive to the chemical composition of the raw water. However, it is to observe that the system Fe^{3+}/*hv* in the presence of model NOM at near neutral pH considerably enhances bacterial photo-inactivation.

4.4.3. Photo-inactivation in simultaneous presence of $Fe^{2+\text{ or }3+}$, H_2O_2 and model NOM (Fig. 5 and Table 2, systems I and III)

The photo-Fenton system in the presence of resorcinol in MilliQ water showed the highest performance and achieved simultaneously to bacterial inactivation a TOC abatement of 90%. Note that even though H_2O_2 concentrations were higher than in the previous experiments with MilliQ water in the absence of resorcinol, synergistic factors were still above 1 (Table 3).

The bacterial inactivation in these systems probably results from a combined action of different pathways as we discussed previously for the experiments in MilliQ water: (i) Endogenous photosensitization; (ii) a synergistic effect of H_2O_2 and *hv* (attack of bacterial membrane, diffusion into the cells and disruption of the intracellular Fe^{2+} balance, leading to intracellular dark Fenton reactions and DNA attack by $^{\bullet}OH$); (iii) a synergistic effect of the presence of Fe^{2+} and *hv* (diffusion into the cell and intracellular dark Fenton reaction with metabolic H_2O_2); (iv) a synergistic effect of the presence of Fe^{3+} and *h* v (classical photo-Fenton reactions in the bulk via the photosensitization of Fe^{3+}-hydroxy complexes or directly on the bacterial surface via the photosensitization of Fe^{3+}-bacteria bounds); (iv) a synergistic effect of the presence of $Fe^{2+\text{ or }3+}$, H_2O_2 and *hv* (classical Fenton and photo-Fenton reactions).

Additionally, as discussed in the previous paragraph, the photo-Fenton process could be strongly enhanced by the presence of resorcinol and its degradation intermediates (i.e. carboxylates) by forming photoactive complexes with iron (i.e. exogenous photosensitization of Fe^{3+}-resorcinol complexes). Moreover, resorcinol or its byproducts could partially substitute the OH groups in Fe^{3+}-hydroxy complexes and stabilize these complexes at near neutral pH. The higher iron concentrations (for both Fe^{2+} and Fe^{3+}) in the suspension after filtration (Fig. 7) compared to iron measured in the same system for MilliQ water only, indicates that the presence of resorcinol does have a chelating effect, in particular during the first step of the experiment. After 60 min, TOC decreases, indicating that resorcinol is subsequently mineralized. Simultaneously, measured iron in the suspensions after filtration also decreases, because the organics ligands are oxidized and loose their ability to chelate iron. Consequently Fe^{3+}-bacteria aggregates which are eliminated by filtration, become predominant over Fe^{3+}-organo complexes.

The positive effect of NOM constituents on photo-Fenton systems, which allows to work at near neutral pH has been reported previously [22,36,37,21,24]. The addition of H_2O_2 to the irradiated Fe^{2+}/Fe^{3+}/organo/*hv* system naturally enhances its efficiency because of the increased production of $^{\bullet}OH$ and the faster Fe^{2+}/Fe^{3+} cycling [75]. Therefore the $Fe^{2+\text{ or }3+}$/H_2O_2(/NOM)/*hv* system becomes particularly interesting for solar disinfection of drinking water sources. Not only present NOM would increase the disinfection performances of the system at near neutral pH, but also the chelating NOM itself is oxidized during a subsequent step in the process [36]. Thus, this system would allow, not only to considerably speed-up SODIS and limit its temperature-dependency, but also to simultaneously degrade NOM. Note that NOM is often responsible for light scattering and post-irradiation bacterial regrowth in conventional solar water disinfection.

4.5. Iron distribution between different compartments of the suspension

To support the suggestion of iron uptake in or deposition on bacteria, we measured the ratio of iron in both, the bacterial pellet and the bulk of the solution for experimental systems prepared with MilliQ only, MilliQ with small quantities of NaCl/KCl and MilliQ containing trypton or resorcinol (Table 4).

4.5.1. Iron accumulation in the bacterial pellet suspended in MilliQ water

In MilliQ 40% of total added iron was accumulated in the bacterial pellet for both systems, containing either Fe^{2+} or Fe^{3+}. In the presence of Fe^{2+}/H_2O_2, this value was of almost 100% and only 45% for the system Fe^{3+}/H_2O_2 (Table 4). Probably in the absence of H_2O_2, Fe^{2+} diffuse into the cells helped by osmotic forces in MilliQ water. Fe^{3+} binds with or deposits on the bacterial membranes proteins and their carboxylic endgroups, but due to their higher charge density, Fe^{3+} ions cannot freely diffuse into the cells. After addition of H_2O_2, the permeability of the membrane increases and Fe^{2+} can diffuse into the cells. Also the roughness of the membrane increases and Fe^{2+} can be transformed to Fe^{3+}. whereafter deposition of Fe^{3+} on the bacterial surface can take place rapidly. Simultaneously, H_2O_2 can modify the outer membrane favoring deposition of Fe^{3+} or enhancing the permeability of the membrane for Fe^{2+}. The sum of the initial Fe^{2+} diffusion and the subsequent Fe^{3+} deposition leads to the almost 100% accumulation of iron in

Table 4
Iron in the bacterial pellet as % from total iron (1 mg L^{-1}). Bacteria were harvested during stationary growth phase, washed and resuspended in either MiliQ water, a 1% (w/w) Bacto™ Trypton solution or in a saline solution, dissolved in the reactors and exposed to simulated sunlight (*h* v). After irradiation, 50 mL were withdrawn. 5 mL were used to determine the total iron concentration and the rest was centrifuged (5000 × *g*, 20 min, 4 °C). 40 mL of the supernate were used to determine the concentration in the matrix. The remaining 5 mL were used to resuspend the bacterial pellet. Measured iron concentrations were then volume corrected. Iron was measured either by the Ferrozine method (first two lines) or by atomic absorption. The table shows the iron accumulation in the bacterial pellet in percent (%) of the total iron.

Suspension matrix	Additives			
	Fe^{2+}, H_2O_2 (**I**)	Fe^{2+} (**II**)	Fe^{3+}, H_2O_2 (**III**)	Fe^{3+} (**IV**)
Saline [a]	90	–	–	–
Trypton [b]	35	–	–	–
MiliQ [c]	95	40	–	–
Trypton [d]	25	20	–	–
MiliQ [c]	97	40	45	40
Resorcinol [e]	30	–	–	–

[a] 120 min irradiation, 1 mg L^{-1} of iron, 10^9 CFU mL^{-1}, 0.8 g NaCl L^{-1}, 0.08 g KCl L^{-1}, 30 mg H_2O_2 L^{-1}. Measurement of iron by the Ferrozine method after digestion.
[b] 120 min of irradiation, 1 mg L^{-1} of iron, 10^9 CFU mL^{-1}, 1 g trypton L^{-1}, 30 mg H_2O_2 L^{-1}. Measurement of iron by the Ferrozine method after digestion.
[c] 45 min of irradiation, 1 mg L^{-1} of iron, 10^8 CFU mL^{-1}, 20 mg H_2O_2 L^{-1}. Measurement of iron by atomic absorption.
[d] 45 min of irradiation, 1 mg L^{-1} of iron, 10^8 CFU mL^{-1}, 1 g trypton L^{-1}, 20 mg H_2O_2 L^{-1}. Measurement of iron by atomic absorption.
[e] 45 min of irradiation, 1 mg L^{-1} or iron, 10^8 CFU mL^{-1}, 60 mg resorcinol L^{-1}, 20 mg H_2O_2 L^{-1}. Measurement of iron by atomic absorption.

the bacterial pellet. The rate for the transformation of Fe^{3+} to Fe^{2+} is considerably slower and consequently, the accumulation of the added $Fe^{2+\text{ or }3+}$ in the bacterial pellet is not significantly different in the presence or absence of H_2O_2.

We already discussed that bacterial cell walls do display a strong affinity for aqueous metal cations, leading to metal surface complexes [75,84]. Fe^{2+}, due to its lower charge density can move more freely as a solute in and out the cells [68]. Fe^{3+} has a higher charge density and can only be sequestrated (when required for metabolic activity) with a highly specific two stage transport system, involving specific binding proteins in the outer membrane and siderophores in the cytoplasm [68]. However, in nature, iron-oxides are often found in close association with bacterial cells in aquatic environments (e.g. Fe^{3+} accumulation by bacterial surfaces in water distribution systems leading to clogging) [85]. The deposition of Fe^{3+} in the presence of bacteria may arise from enzymatic mechanisms that brings about the secretion of binding proteins and other metabolic iron chelating agents. It may results also from non-enzymatic reactions such as iron chelating on binding proteins and carboxylic endgroups of membrane proteins or by passive adsorption of cationic iron to the surface of microbial cell [28,27,69,70,86].

4.5.2. Iron accumulation in the bacterial pellet in the presence of trypton or resorcinol

In the presence of trypton or resorcinol in the system, iron accumulation in the bacterial pellet is significantly lower for Fe^{2+} whether or not H_2O_2 is present (Table 4). This observation confirms the hypothesis that organics in the solution compete with bacteria for the available iron, leading to the formation of Fe-organo complexes and enhancing iron solubility.

We already suggested that the formation of Fe^{3+}-bacteria complexes is possible and that the irradiation of such complexes can lead to bacterial inactivation. We have also discussed, how the presence of organic matter hinders the interaction of $Fe^{2+\text{ or }3+}$ and bacteria, but does not affect the overall efficiency of the photo-Fenton systems, due to the formation of Fe^{3+}-organo complexes and their sensitization by UVA and visible light. The bactericidal effect of Fe^{2+} for *E. coli*, is an interesting observation. However, natural waters are normally oxygenated and the natural Fe^{2+} concentrations are generally insignificant. Further, in the absence of enhanced osmotic pressure, the diffusion of Fe^{2+} into cells is limited. Fe^{3+} is often naturally present in raw water sources and Fe^{3+}/bacteria/organo/*hv* systems are highly promising not only because of the considerable enhancement of solar water disinfection for *E. coli* at near neutral pH, but also because they allow the simultaneous elimination of NOM.

4.6. Mechanistic interpretation

Based on the experimental results and a critical revision of literature, a mechanistic interpretation of the inactivation of *E. coli* in the presence of Fe^{2+}, Fe^{3+}, H_2O_2 and the photo-Fenton reagent ($Fe^{2+\text{ or }3+}/H_2O_2$) under solar radiation (*hv*) is suggested. An overview is presented in Fig. 8.

The processes are subdivided in two groups. The first group concerns processes leading to increased generation of ROS in the systems (**a** –**j**). The second category concerns the way of how these reactive species affect the viability of *E. coli* (**1** and **2**). Indeed, additional mechanisms are probably taking place in reality and for those suggested here, rate constants were not quantified. However, the presented mechanistic interpretation suggests a comprehensive overview of the probably most relevant processes and pathways involved in iron-catalyzed solar water disinfection.

4.6.1. Sources of ROS and cellular photo-oxidative stress

(a) Enzymes like catalase or sodium dismutase (SOD), responsible for the elimination of metabolic generated H_2O_2 and $O_2^{\bullet-}$, can

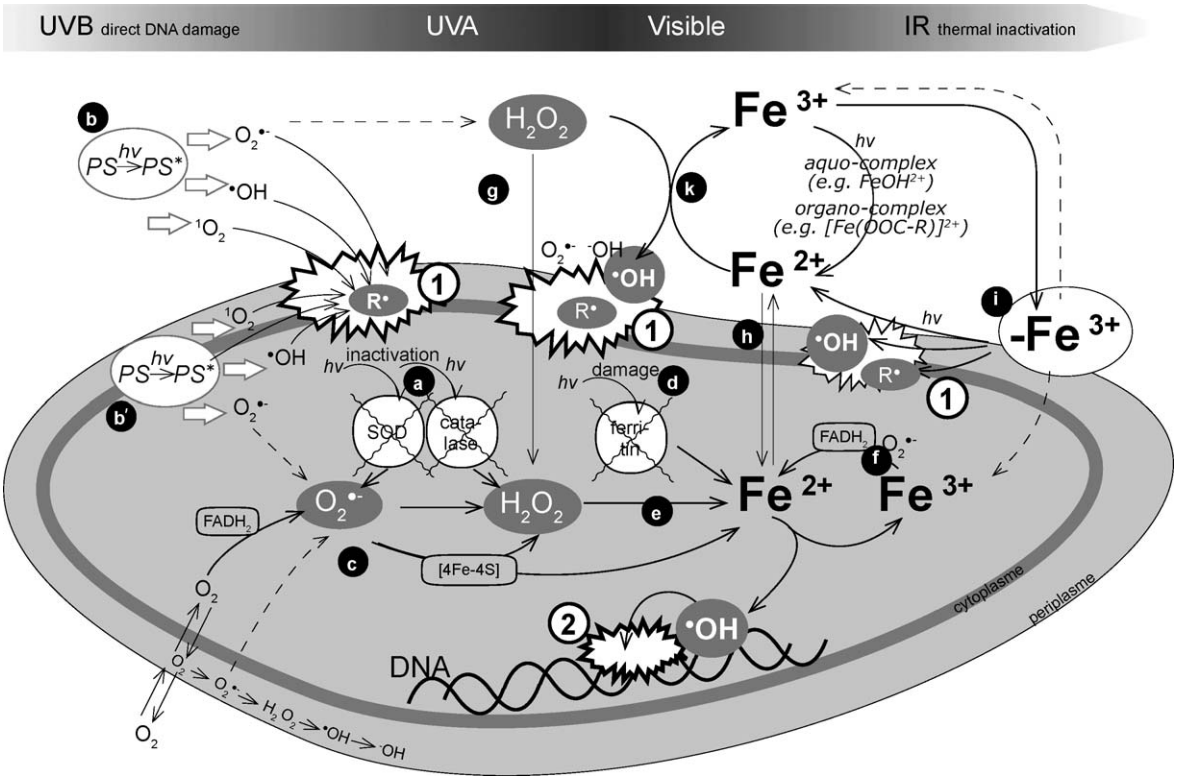

Fig. 8. Possible pathways involved in photo-inactivation of *E. coli* **in the presence of** Fe^{2+}, Fe^{3+}**and** H_2O_2. Sources of ROS and cellular photo-oxidative stress (**a** –**j**) and cellular damage caused by ROS (**1** and **2**). Further explanations are given in the text (Section 4.6).

be damaged by near UVA light. Their dysfunction can lead to increased intracellular concentrations of long living ROS like H_2O_2 and $O_2^{\bullet-}$ [6,29].

(b) Endogenous and exogenous photosensitizers absorb light in the UVA and visible spectrum. The excited PS can either directly attack biomolecules or react with surrounding oxygen generating ROS such as $^1O2$, $O_2^{\bullet-}$, $^{\bullet}OH$ and H_2O_2 [3,7,4].

(c) Auto-oxidation of cellular flavoproteins ($FADH_2$) can generate a mixture of cellular $O_2^{\bullet-}$ and H_2O_2. $O_2^{\bullet-}$ can oxidize cellular iron-sulfur clusters ([4Fe-4S]), causing inactivation of the bearing proteins, release of Fe^{2+} and generation of H_2O_2 [50,8].

(d) UVA light can damage iron containing proteins such as ferritin, leading to the intracellular release of Fe^{2+}[58,59].

(e) Intracellular H_2O_2 can react with free or loosely bound Fe^{2+} via the Haber–Weiss reaction, generating highly toxic $^{\bullet}OH$ [53].

(f) $O_2^{\bullet-}$, $FADH_2$ or NAD(P)H can be an effective electron donor and reducing agent for the regeneration of Fe^{2+} from Fe^{3+} inside the cells [62,26,50].

(g) H_2O_2 is a long living ROS, thus relatively stable (unlike $^{\bullet}OH$) and uncharged (unlike $O_2^{\bullet-}$). When added to the bulk, H_2O_2 penetrates the bacterial membrane and diffuses into cells [6,29].

(h) Added Fe^{2+} has a lower charge density than Fe^{3+} and can diffuse freely into the cells. This diffusion is enhanced by a favorable osmotic forces present in MilliQ water.

(i) Added Fe^{3+} in the bulk of the suspension cannot move freely into the cells. Fe^{3+} can be adsorbed on specific binding proteins, which manage its transport inside the cell for facultative anaerobic respiration via siderophores (metabolic Fe^{3+} chelating agents) in the cytoplasm [68]. Fe^{3+} might also binds on other proteins of the bacterial membrane and their carboxylic endgroups. The deposition of Fe^{3+} on bacterial cells might lead to the formation of Fe^{3+}-bacteria exciplexes. The photosensitization of these bounds in the near UVA and visible spectrum could lead to direct oxidation of the membrane, initiation of lipid peroxidation chains and the generation of Fe^{2+} and $^{\bullet}OH$ in spitting distance of the target microorganism [28,27,34,69,70].

(j) Extracellular Fe^{2+} is oxidized to H_2O_2 via Haber–Weiss (Eq. (1)) leading to the formation of highly reactive, short living, $^{\bullet}OH$ and other ROS in the bulk. Photo-active Fe^{3+}-organo and -hydroxy complexes can absorb UVA and visible light, leading to the regeneration of Fe^{2+} and the formation of additional ROS in the bulk via the photo-Fenton reagent [28]. The formation of Fe^{3+}-organo and -hydroxy complexes allows the photo-Fenton reactions to take place at near neutral pH [27,34,36,37,22]. Especially the Fe^{3+}-organo are generally stable at near neutral pH and show higher light absorption in the solar visible light range than hydroxy complexes.

4.6.2. Cellular damage caused by reactive oxygen species (ROS)

(1) ROS will react with cellular constituents such as proteins and cell membrane components (i.e. lipids), leading to the initiation of lipid peroxidation chains inside the cells and at the cellular membrane leading to enhanced permeability and inactivation [52,51,4].

(2) The highly reactive radical $^{\bullet}OH$ is the only oxygen species, which can directly damage DNA [55] and no cellular defense mechanism against this attack has been identified until today [55]. $^{\bullet}OH$ reacts with whatever is present at its site of formation close to a diffusion-controlled rate, are therefore short living. Therefore $^{\bullet}OH$ needs to be formed close to its target for being effective. $^{\bullet}OH$ formed close to DNA (e.g. on Fe^{2+} associated with DNA) attack occur at the DNA bases or sugars leading to strand breakage and base release [53,54,58,61].

5. Conclusions

Solar photo-Fenton systems at low concentrations of reagent (0.6 mg L^{-1} of $Fe^{2+\text{ or }3+}$ and 10 mg L^{-1} H_2O_2) and at near neutral pH were efficient for both, bacterial inactivation and the mineralization of model organic matter. Based on a systematic laboratory study, a mechanistic overview of possible pathways leading to iron-catalyzed photo-inactivation was suggested.

The photo-Fenton ($Fe^{2+\text{ or }3+}/H_2O_2/h\nu$) was the most efficient experimental systems for bacterial photo-inactivation in all, MilliQ water, water containing inorganic ions (mineral water) and MilliQ water enriched with model NOM (resorcinol). While the system $Fe^{2+}/H_2O_2/h$ v showed a better performance in MilliQ water compared to the system $Fe^{3+}/H_2O_2/h\nu$, the latter was superior in the presence of inorganic ions or model organic matter.

The system $H_2O_2/h\nu$ had also a beneficial effect for bacterial inactivation (except in the presence of inorganic ions) and the presence of residual H_2O_2 in bacterial suspension during post-irradiation storage inhibited regrowth. H_2O_2 and light ($h\nu$) showed a synergistic effect because the cellular antioxidants system is affected by UVA and visible light leading to increased intracellular concentrations of H_2O_2. Excessive H_2O_2 reacts with free or loosely bound intracellular Fe^{2+} via the Haber–Weiss reaction to form highly toxic $^{\bullet}OH$ (intracellular dark Fenton). This effect was apparently sufficient to provoke bacterial inactivation even in post-irradiation dark storage. Therefore, it might be interesting to assess the low-cost availability of H_2O_2 for a real scale application (e.g. tablets, electrochemical *in situ* generation). However, as the long term health effects of H_2O_2 for human consumption are not yet well known, residual concentrations at the point of consumption should be negligible.

Fe^{2+} alone did enhance bacterial inactivation under irradiation and in the dark. This was associated with an excessive diffusion of Fe^{2+} into the cells due to favorable osmotic pressure in MilliQ water. Intracellular Fe^{2+} can react with intracellular H_2O_2 (which is always produced in respiration) and form toxic $^{\bullet}OH$. In naturally oxygenated water, Fe^{2+} is not predominant. However, when iron needs to be added, a system where Fe^{2+} is generated *in situ* from zerovalent iron, as it is already implemented for the elimination of arsenic from drinking water could be interesting.

Fe^{3+} alone did enhance bacterial inactivation under irradiation only ($Fe^{3+}/h\nu$). This was associated with either the formation of photoactive Fe^{3+}-organo complexes allowing photo-Fenton reactions at near neutral pH in the bulk (in the presence of resorcinol) or the deposition of Fe^{3+} on the bacterial membrane. The so formed Fe^{3+}-bacteria bound could (or organo-Fe^{3+}-bacteria aggregates) undergo photosensitization leading to the production of reactive species close to the bacterial surfaces and direct oxidation of cellular components. Moreover, resorcinol or its degradation byproducts could partially substitute the OH groups in Fe^{3+}-hydroxy complexes and stabilize these complexes at near neutral pH. This observation is of particular interest because Fe^{3+} as well as NOM is often naturally present in raw drinking water and certainly explains the fast inactivation rates observed for iron-catalyzed disinfection in our previous works with natural raw water.

While model organic matter had a beneficial effect on iron-catalyzed solar water disinfection, inorganic ions showed an inhibitory effect in our experiments. This illustrates the main problem often faced in the development of low-cost water treatment technologies as the efficiency of such treatment systems at real scale varies strongly with the chemical characteristics of drinking water sources.

The Fenton reagent as an additive in the solar water disinfection treatment would limit the required exposure time and radiation

intensity and allow the simultaneous degradation of chemical pollutants (e.g. pesticides, other organic xenobiotics, arsenic) and NOM. Due to the accelerated bacterial inactivation and temperature independence, iron-catalyzed SODIS systems could be developed with more liberty regarding the shape and volume of reactors or the local climate, limit the risk for post-irradiation regrowth, facilitate the acceptance among target populations and allow a larger dissemination of this sustainable low-cost technology.

Safe drinking water is a key factor for health and consequently the social and economic development. The improvement of solar water disinfection contributes to the development of simple and low-cost household level drinking water treatments, which are economically, socially and environmentally sustainable.

Acknowledgements

The authors thank C. Roussel and S. Thonney for the measurement done at the Institute of Chemical Science and Engineering (ISIC) at the EPFL. The authors thank the Environmental Microbiology Laboratory at the EPFL to provide for laboratory facilities.

References

[1] WHO, Combating Waterborne Disease at the Household Level (The International Network to Promote Household Water Treatment and Safe Storage), WHO, Geneva, Switzerland, 2007.
[2] M. Wegelin, S. Canonica, K. Mechsner, T. Fleischmann, F. Pesaro, A. Metzler, Solar water disinfection: scope of the process and analysis of radiation experiments, J. Water Supply Res. Technol. AQUA 43 (4) (1994) 154–169.
[3] A. Acra, M. Jurdi, H. Mu'allem, Y. Karahagopian, Z. Raffoul, Water Disinfection by Solar Radiation: Assessment and Application, International Development Research Centre (IDRC – Canada), PO Box 8500, Ottawa, Ont., Canada K1G 3H9, 1990.
[4] R.H. Reed, The inactivation of microbes by sunlight: solar disinfection as a water treatment process, Adv. Appl. Microbiol. 54 (2004) 333–365.
[5] B. Sommer, A. Marino, Z. Solarte, M.L. Salas, C. Dierolf, C. Valiente, D. Morat, R. Rechsteiner, P. Setter, W. Wirojanagud, H. Ajarmeh, A. Al-Hassan, M. Wegelin, SODIS- an emerging water treatment process, J. Water Supply Res. Technol. AQUA 46 (3) (1997) 127–137.
[6] P.S. Hartman, A. Eisenstark, Synergistic killing of Escherichia coli by near-UV radiation and hydrogen peroxide: distinction between recA-repairable and recA-nonrepairable damage, J. Bacteriol. 133 (2) (1978) 769–774.
[7] T. Kohn, K.L. Nelson, Sunlight-mediated Inactivation of MS2 Coliphage via exogenous singlet oxygen produced by sensitizers in natural waters, Environ. Sci. Technol. 41 (1) (2007) 192–197.
[8] E.S. Henle, S. Linn, Formation, prevention, and repair of DNA damage by iron/hydrogen peroxide, J. Biol. Chem. 272 (31) (1997) 19095–19098.
[9] K.G. McGuigan, T.M. Joyce, R.M. Conroy, Solar disinfection: use of sunlight to decontaminate drinking water in developing countries, J. Photochem. Photobiol. A 64 (2) (1999) 785–787.
[10] D. Mäusezahl, A. Christen, G.D. Pacheco, F.A. Tellez, M. Iriarte, M.E. Zapata, M. Cevallos, J. Hattendorf, M.D. Cattaneo, B. Arnold, T.A. Smith, J.M. Colford Jr., Solar drinking water disinfection (SODIS) to reduce childhood diarrhoea in rural bolivia: a cluster-randomized, controlled trial, PLoS Med. 6 (8) (2009) e1000125.
[11] S.C. Kehoe, T.M. Joyce, P. Ibrahim, J.B. Gillespie, R.A. Shahar, K.G. McGuigan, Effect of agitation, turbidity, aluminium foil reflectors and container volume on the inactivation efficiency of batch-process solar disinfectors, Water Res. 35 (4) (2001) 1061–1065.
[12] A.G. Rincón, C. Pulgarin, N. Adler, P. Peringer, Interaction between *E. coli* inactivation and DBP-precursors—dihydroxybenzene isomers—in the photocatalytic process of drinking-water disinfection with TiO_2, J. Photochem. Photobiol. A 139 (2–3) (2001) 233–241.
[13] E.F. Duffy, F.A. Touati, S.C. Kehoe, O.A. McLoughlin, L.W. Gill, W. Gernjak, I. Oller, M.I. Maldonado, S. Malato, J. Cassidy, R.H. Reed, K.G. McGuigan, A novel TiO_2-assisted solar photocatalytic batch-process disinfection reactor for the treatment of biological and chemical contaminants in domestic drinking water in developing countries, Sol. Energy 77 (5) (2004) 649–655.
[14] J. Lonnen, S. Kilvingtona, S. Kehoe, F. Al-Touati, K. McGuigan, Solar and photocatalytic disinfection of protozoan, fungal and bacterial microbes in drinking water, Water Res. 39 (2005) 877–883.
[15] A.-G. Rincón, C. Pulgarin, Use of coaxial photocatalytic reactor (CAPHORE) in the TiO_2 photo-assisted treatment of mixed *E. coli* and Bacillus sp. and bacterial community present in wastewater, in: Environmental Applications of Photocatalysis, 3rd European Meeting on Solar Chemistry and Photocatalysis: Environmental Applications, Catal. Today 101 (3–4) (2005) 331–344.
[16] J. Marugán, R. van Grieken, C. Sordo, C. Cruz, Kinetics of the photocatalytic disinfection of *Escherichia coli* suspensions, Appl. Catal. B 82 (1–2) (2008) 27–36.
[17] M. Cho, Y. Lee, H. Chung, J. Yoon, Inactivation of *Escherichia coli* by photochemical reaction of ferrioxalate at slightly acidic and near-neutral pHs, Appl. Environ. Microbiol. 70 (2) (2004) 1129–1134.
[18] A.G. Rincón, C. Pulgarin, Comparative evaluation of Fe^{3+} and TiO_2 photoassisted processes in solar photocatalytic disinfection of water, Appl. Catal. B 63 (3–4) (2006) 222–231.
[19] A.-G. Rincón, C. Pulgarin, Absence of E. coli regrowth after Fe^{3+} and TiO_2 solar photoassisted disinfection of water in CPC solar photoreactor, Catal. Today 124 (3-4) (2007) 204–214.
[20] A.-G. Rincón, C. Pulgarin, Fe^{3+} and TiO_2 solar-light-assisted inactivation of *E. coli* at field scale: implications in solar disinfection at low temperature of large quantities of water, Catal. Today 122 (1–2) (2007) 128–136.
[21] A. Moncayo-Lasso, J. Sanabria, C. Pulgarin, N. Benítez, Simultaneous *E. coli* inactivation and NOM degradation in river water via photo-Fenton process at natural pH in solar CPC reactor. A new way for enhancing solar disinfection of natural water, Chemosphere 77 (2) (2009) 296–300.
[22] C.A. Murray, S.A. Parsons, Removal of NOM from drinking water: Fenton's and photo-Fenton's processes, Chemosphere 54 (7) (2004) 1017–1023.
[23] A. Moncayo-Lasso, C. Pulgarin, N. Benítez, Degradation of DBP's precursors in river water before and after slow sand filtration by photo-Fenton process at pH 5 in a solar CPC reactor, Water Res. 42 (15) (2008) 4125–4132.
[24] A.W. Vermilyea, B.M. Voelker, Photo-Fenton reaction at near neutral pH, Environ. Sci. Technol. 43 (2009) 6927–6933.
[25] F. Haber, J. Weiss, The catalytic decomposition of hydrogen peroxide by iron salts, Proc. R. Soc. Lond. Ser. A 147 (861) (1934) 332–351.
[26] A. Sychev, V. Isak, Iron compounds and the mechanisms of the homogeneous catalysis of the activation of O_2 and H_2O_2 and of the oxidaiton of organic substrates, Russian Chem. Rev. 65 (1995) 1105–1129.
[27] A. Safarzadeh-Amiri, J.R. Bolton, S.R. Cater, The use of iron in advanced oxidation processes, J. Adv. Oxidation Technol. 1 (1) (1996) 18–26.
[28] J.J. Pignatello, E. Oliveros, A. MacKay, Advanced oxidation processes for organic contaminant destruction based on the Fenton reaction and related chemistry, Crit. Rev. Environ. Sci. Technol. 36 (1) (2006) 1–84.
[29] J.A. Imlay, Cellular defenses against superoxide and hydrogen peroxide, Annu. Rev. Biochem. 77 (1) (2008) 755–776.
[30] C. Walling, A. Goosen, Mechanism of the ferric ion catalyzed decomposition of hydrogen peroxide. Effect of organic substrates, J. Am. Chem. Soc. 95 (9) (1973) 2987–2991, 120 cited By (since 1996).
[31] J.D. Laat, H. Gallard, Catalytic decomposition of hydrogen peroxide by Fe(III) in homogeneous aqueous solution: mechanism and kinetic modeling, Environ. Sci. Technol. 33 (1999) 2726–2732.
[32] W. Gernjak, M. Fuerhacker, P. Fernández-Ibánez, J. Blanco, S. Malato, Solar photo-Fenton treatment—process parameters and process control, Appl. Catal. B 64 (1–2) (2006) 121–130, cited by (since 1996) 25.
[33] B.C. Faust, J. Hoigné, Photolysis of Fe(III)-hydorxy complexes as sources of OH radicals in clouds, fogs and rains, Atmos. Environ. 24A (1) (1990) 79–89.
[34] W. Feng, D. Nansheng, Photochemistry of hydrolytic iron(III) species and photoinduced degradation of organic compounds. A minireview, Chemosphere 41 (8) (2000) 1137–1147.
[35] R.G. Zepp, B.C. Faust, J. Hoigné, Hydroxyl radical formation in aqueous reactions (pH 3–8) of iron(II) with hydrogen peroxide: the photo-Fenton reaction, Environ. Sci. Technol. 26 (2) (1992) 313–319.
[36] A. Georgi, A. Schierz, U. Trommler, C. Horwitz, T. Collins, F.-D. Kopinke, Humic acid modified Fenton reagent for enhancement of the working pH range, Appl. Catal. B 72 (1-2) (2007) 26–36.
[37] E. Lipczynska-Kochany, J. Kochany, Effect of humic substances on the Fenton treatment of wastewater at acidic and neutral pH, Chemosphere 73 (5) (2008) 745–750.
[38] S.J. Hug, O. Leupin, Iron-catalyzed oxidation of arsenic(III) by oxygen and by hydrogen peroxide: pH-dependent formation of oxidants in the Fenton reaction, Environ. Sci. Technol. 37 (12) (2003) 2734–2742.
[39] H.F. Diao, X.Y. Li, J.D. Gu, H.C. Shi, Z.M. Xie, Electron microscopic investigation of the bactericidal action of electrochemical disinfection in comparison with chlorination, ozonation and Fenton reaction, Process Biochem. 39 (11) (2004) 1421–1426.
[40] A. Moncayo-Lasso, R.A. Torres-Palma, J. Kiwi, N. Benítez, C. Pulgarin, Bacterial inactivation and organic oxidation via immobilized photo-Fenton reagent on structured silica surfaces, Appl. Catal. B 84 (3–4) (2008) 577–583.
[41] W. Gernjak, T. Krutzler, A. Glaser, S. Malato, J. Caceres, R. Bauer, A. Fernández-Alba, Photo-Fenton treatment of water containing natural phenolic pollutants, Chemosphere 50 (1) (2003) 71–78.
[42] M. Lapertot, C. Pulgarin, P. Fernández-Ibánez, M.I. Maldonado, L. Pérez-Estrada, I. Oller, W. Gernjak, S. Malato, Enhancing biodegradability of priority substances (pesticides) by solar photo-Fenton, Water Res. 40 (5) (2006) 1086–1094.
[43] O. Leupin, S. Hug, A. Badruzzaman, Arsenic removal from Bangladesh tube well water with filter columns containing zerovalent iron filings and sand, Environ. Sci. Technol. 39 (20) (2005) 8032–8037.
[44] M. Biterna, L. Antonoglou, E. Lazou, D. Voutsa, Arsenite removal from waters by zero valent iron: batch and column tests, Chemosphere 78 (1) (2010) 7–12.
[45] P. Ribordy, C. Pulgarin, J. Kiwi, P. Péringer, Electrochemical versus photochemical pretreatment of industrial wastewaters, Water Sci. Technol. 35 (4) (1997) 293–302.
[46] E. Viollier, P.W. Inglett, K. Hunter, A.N. Roychoudhury, P.V. Cappellen, The ferrozine method revisited: Fe(II)/Fe(III) determination in natural waters, Appl. Geochem. 15 (6) (2000) 785–790.

[47] L. Stookey, Ferrozine- a new apectrophotometric reagent for iron, Anal. Chem. 42 (7) (1970) 779–781.
[48] K. McGuigan, T. Joyce, R. Conroy, J. Gillespie, M. Elmore-Meegan, Solar disinfection of drinking water contained in transparent plastic bottles—characterizing the bacterial inactivation process, J. Appl. Microbiol. 84 (1998) 1138–1148.
[49] M. Fisher, C. Keenan, K. Nelson, B. Voelker, Speeding up solar disinfection (SODIS): effects of hydrogen peroxide, temperature, pH, and copper plus ascorbate on the photoinactivation of E. coli, J. Water Health 6 (1) (2008) 35–51.
[50] J.A. Imlay, Pathways of oxidative damage, Annu. Rev. Microbiol. 57 (1) (2003) 395–418.
[51] M. Gourmelon, J. Cillard, M. Pommepuy, Visible light damage to *Escherichia coli* in seawater: oxidative stress hypothesis, J. Appl. Microbiol. 77 (1) (1994) 105–112.
[52] E. Cabiscol, J. Tamarit, J. Ros, Oxidative stress in bacteria and protein damage by reactive oxygen species, Int. Microbiol. 3 (1) (2000) 3–8.
[53] B. Halliwell, O.I. Aruoma, DNA damage by oxygen-derived species. Its mechanism and measurement in mammalian systems, FEBS Lett. 281 (1-2) (1991) 9–19.
[54] B. Halliwell, J.M. Gutteridge, Biologially relevant metal ion-dependent hydroxyl radical generation, FEBS Lett. 307 (1) (1992) 108–112.
[55] U. Sattler, P. Calsou, S. Boiteux, B. Salles, Detection of oxidative base DNA damage by a new biochemical assay, Arch. Biochem. Biophys. 376 (1) (2000) 26–33.
[56] R. Reed, S. Mani, V. Meyer, Solar photo-oxidative disinfection of drinking water: preliminary field observations, Lett. Appl. Microbiol. 30 (6) (2000) 432–436.
[57] S. Malato, P. Fernández-Ibánez, M. Maldonado, J. Blanco, W. Gernjak, Decontamination and disinfection of water by solar photocatalysis: recent overview and trends, Catal. Today 147 (1) (2009) 1–59.
[58] J. Hoerter, A. Pierce, C. Troupe, J. Epperson, A. Eisenstark, Role of enterobactin and intracellular iron in cell lethality during near-UV irradiation in *Escherichia coli*, Photochem. Photobiol. 64 (3) (1996) 537–541.
[59] R. Tyrrell, C. Pourzand, J. Brown, V. Hejmadi, E. Kvam, S. Ryter, R. Watkin, Cellular studies with UVA radiation: a role for iron, Radiat. Prot. Dosim. 91 (1–3) (2000) 37–39.
[60] I. Fridovich, Superoxide radical and superoxide dismutases, Annu. Rev. Biochem. 64 (1995) 97–112.
[61] Y. Luo, Z. Han, S. Chin, S. Linn, Three chemically distinct types of oxidants formed by iron-mediated Fenton reactions in the presence of DNA, Proc. Natl. Acad. Sci. U. S. A. 91 (26) (1994) 12438–12442.
[62] A. Eisenstark, Bacterial gene products in response to near-ultraviolet radiation, Mutat. Res. 422 (1998) 85–95.
[63] E. Tytler, T. Wong, G. Codd, Photoinactivation in vivo of superoxide dismutase and catalase in the cyanobacterium *Microcystis aeruginosa*, FEMS Microbiol. Lett. 23 (2-3) (1984) 239–242.
[64] J.M. Gutteridge, The role of superoxide and hydroxyl radicals in phospholipid peroxidation catalysed by iron salts, FEBS Lett. 150 (2) (1982) 454–458.
[65] C. Sichel, P. Fernández-Ibánez, M. de Cara, J. Tello, Lethal synergy of solar UV-radiation and H_2O_2 on wild Fusarium solani spores in distilled and natural well water, Water Res. 43 (7) (2009) 1841–1850.
[66] J.A. Imlay, S. Linn, DNA damage and oxygen radical soxicity, Science 240 (4857) (1988) 1302–1309.
[67] D. Touati, Iron and Oxidative stress in bacteria, Arch. Biochem. Biophys. 373 (1) (2000) 1–6.
[68] V. Braun, Iron uptake mechanisms and their regulation in pathogenic bacteria, Int. J. Med. Microbiol. 291 (2) (2001) 67–79.
[69] B.C. Faust, R.G. Zepp, Photochemistry of aqueous iron(III)-polycarboxylate complexes: roles in the chemistry of atmospheric and surface waters, Environ. Sci. Technol. 27 (1993) 2517–2522.
[70] Y. Zuo, J. Hoigné, Formation of hydrogen peroxide and depletion of oxalic acid in atmospheric water by photolysis of iron(III)-oxalato complexes, Environ. Sci. Technol. 26 (1992) 1014–1022.
[71] C. Catastini, M. Sarakha, G. Mailhot, M. Bolte, Iron(III) aquacomplexes as effective photocatalysts for the degradation of pesticides in homogeneous aqueous solutions, Sci. Total Environ. 298 (2002) 219–228.
[72] G. Mailhot, M. Sarakha, B. Lavedrine, J. Cáceres, S. Malato, Fe^{3+}-solar light induced degradation of diethyl phthalate (DEP) in aqueous solutions, Chemosphere 49 (6) (2002) 525–532.
[73] D.T. Sawyer, J.S. Valentine, How super is superoxide? Acc. Chem. Res. 14 (1981) 292–400.
[74] V. Sarria, M. Deront, P. Péringer, C. Pulgarin, Degradation of a biorecalcitrant dye precursor present in industrial wastewaters by a new integrated iron(III) photo-assisted-biological treatment, Appl. Catal. B 40 (3) (2003) 231–246.
[75] P. Ciesla, P. Kocot, P. Mytych, Z. Stasicka, Homogeneous photocatalysis by transition metal complexes in the environment, J. Mol. Catal. A: Chem. 224 (1-2) (2004) 17–33.
[76] A.-G. Rincón, Effect of pH, inorganic ions, organic matter and H_2O_2 on *E. coli* K12 photocatalytic inactivation by TiO_2: implications in solar water disinfection, Appl. Catal. B 51 (4) (2004) 283–302.
[77] A.G. Rincon, C. Pulgarin, Solar photolytic and photocatalytic disinfection of water at laboratory and field scale. Effect of the chemical composition of water and study of the post-irradiation events, J. Sol. Energy Eng. 129 (2007) 100–110.
[78] P. Fernández-Ibánez, C. Sichel, M. Polo-López, M. de Cara-Garca, J. Tello, Photocatalytic disinfection of natural well water contaminated by Fusarium solani using TiO_2 slurry in solar CPC photo-reactors, Catal. Today 144 (1-2) (2009) 62–68.
[79] G. Gogniat, M. Thyssen, M. Denis, C. Pulgarin, S. Dukan, The bactericidal effect of TiO_2 photocatalysis involves adsorption onto catalyst and the loss of membrane integrity, FEMS Microbiol. Lett. 258 (1) (2006) 18–24.
[80] J. Kochany, E. Lipczynska-Kochany, Application of the EPR spin-trapping technique for the investigation of the reactions of carbonate, bicarbonate, and phosphate anions with hydroxyl radicals generated by the photolysis of H_2O_2, Chemosphere 25 (12) (1992) 1769–1782.
[81] T.G. Aldsworth, C.E.R. Sharman, Dodd, Bacterial suicide through stress, Cell. Mol. Life Sci. 56 (1999) 378–383.
[82] F. Bosshard, M. Berney, M. Scheifele, H.-U. Weilenmann, T. Egli, Solar disinfection (SODIS) and subsequent dark storage of *Salmonella typhimurium* and *Shigella flexneri* monitored by flow cytometry, Microbiology 155 (4) (2009) 1310–1317.
[83] R. Khaengraeng, R. Reed, Oxygen and photoinactivation of *Escherichia coli* in UVA and sunlight, J. Appl. Microbiol. 99 (1) (2005) 39–50.
[84] J.B. Fein, C.J. Daughney, N. Yee, T.A. Davis, A chemical equilibrium model for metal adsorption onto bacterial surfaces, Geochim. Cosmochim. Acta 61 (16) (1997) 3319–3328.
[85] X. Chaterlier, D. Fortin, M.M. West, G.G. Lepard, F.G. Ferris, Effect of the presence of bacterial surfaces during the synthesis of Fe oxides by oxidation of ferrous ions, Eur. J. Miner. 13 (4) (2001) 705–714.
[86] I.C. Macrae, J.F. Edwards, Adsorption of colloidal iron by bacteria, Appl. Environ. Microbiol. 24 (5) (1972) 819–823.